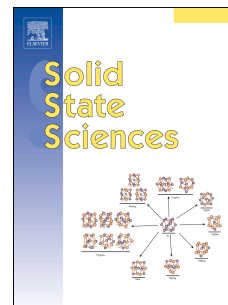


# Journal Pre-proof

Physical genetics: Cross-breeding density functional theory and X-ray photoelectron spectroscopy to rationalize chemical shifts of binding energies in solid compounds

Horst P. Beck, Giuliano Moretti



PII: S1293-2558(20)30338-1

DOI: <https://doi.org/10.1016/j.solidstatesciences.2020.106359>

Reference: SSSCIE 106359

To appear in: *Solid State Sciences*

Received Date: 6 March 2020

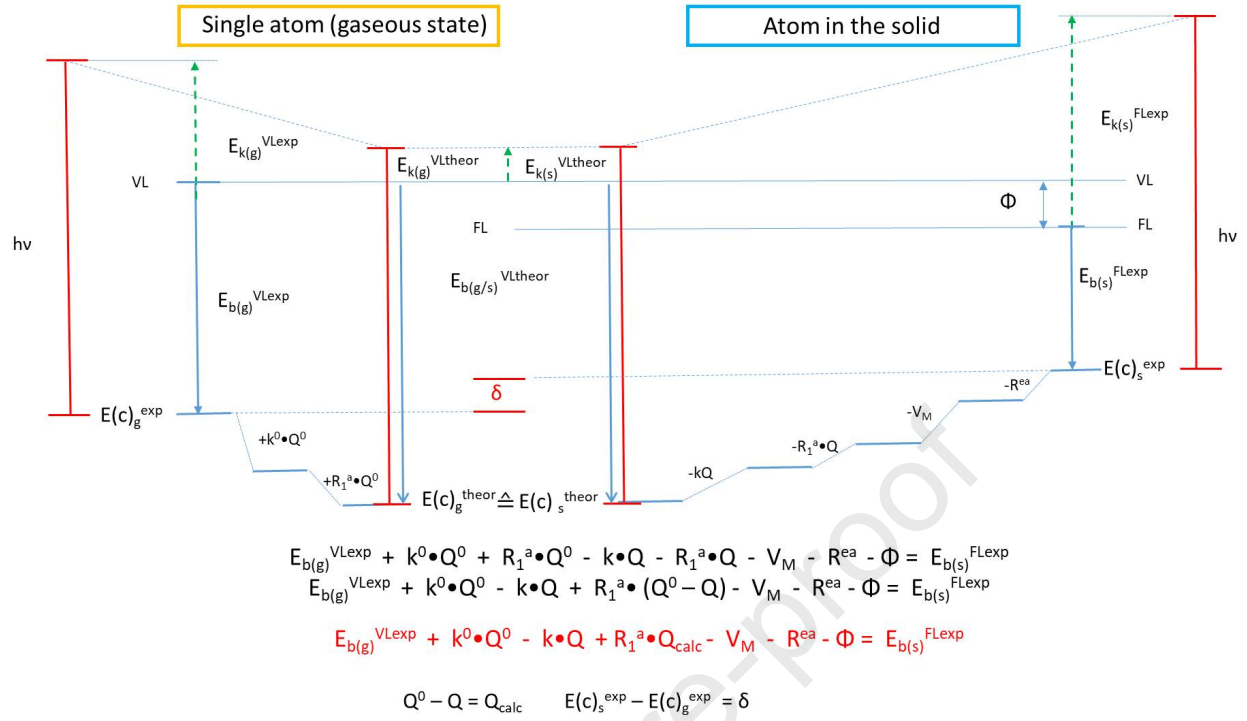
Revised Date: 7 July 2020

Accepted Date: 11 July 2020

Please cite this article as: H.P. Beck, G. Moretti, Physical genetics: Cross-breeding density functional theory and X-ray photoelectron spectroscopy to rationalize chemical shifts of binding energies in solid compounds, *Solid State Sciences* (2020), doi: <https://doi.org/10.1016/j.solidstatesciences.2020.106359>.

This is a PDF file of an article that has undergone enhancements after acceptance, such as the addition of a cover page and metadata, and formatting for readability, but it is not yet the definitive version of record. This version will undergo additional copyediting, typesetting and review before it is published in its final form, but we are providing this version to give early visibility of the article. Please note that, during the production process, errors may be discovered which could affect the content, and all legal disclaimers that apply to the journal pertain.

© 2020 Published by Elsevier Masson SAS.



## Physical genetics: cross-breeding density functional theory and X-ray photoelectron spectroscopy to rationalize chemical shifts of binding energies in solid compounds.

Horst P. Beck<sup>a\*</sup> and Giuliano Moretti<sup>b</sup>

<sup>a)</sup> Fachbereich Chemie der Universität des Saarlandes, Im Stadtwald, 66123 Saarbrücken, Germany

<sup>b)</sup> Dipartimento di Chimica, Università di Roma “La Sapienza”, Piazzale A. Moro 5, 00185 Roma, Italy

\*Corresponding author: Tel.: +49 681 302 2481; fax +49 681 302 4233;

E-mail address: [hp.beck@mx.uni-saarland.de](mailto:hp.beck@mx.uni-saarland.de)

**Keywords** chemical shifts in XPS; Bader charges; initial and final state effects; Wagner plot; relaxation effects;

### Abstract

Like other spectroscopic methods XPS and AES show characteristic chemical shifts depending on the elemental matrix of a compound, however, a satisfactory rationalization of the variance of such values is often difficult. By an extension of a previous approach we present a theory in a unifying equation which combines several parameters - some of them resulting from DFT calculations - which influence the energy of the outgoing electrons and thereby seemingly the binding energy. By calculating Bader charges, atomic volumes and site potentials we have produced a data basis for a set of chalcogenides and halides of Ba, Zn, Pb and Cu to rationalize the spread of measured binding energies and Auger energies. It has thereby become possible to quantify different factors separately which bias the measurement of the kinetic energies of the outgoing core electrons, both the photo-emitted and the Auger electrons. Such an analysis can also trace special features of an open-shell configuration and even show up effects of a semiconductor-type.

### 1 Introduction

X-ray fluorescence (XFS) and X-ray photoelectron spectroscopy (XPS) together with Auger electron spectroscopy (AES) are well known analytical methods to explore the elemental composition of materials. Well tabulated characteristic X-ray or electron energies emitted by the material under inspection allow identifying the various atomic species more or less unambiguously, and the intensity of such emissions may well be used for quantification of the elements after calibration of the respective method. However, when looking up the energies in an atlas of XPS data we do not find discrete data but ranges of values depending on the oxidation state of the elements and of the type of compounds, i.e. the elemental association and the bonding type.

An exact analysis of the kinetic energy of emitted electrons ( $E_k$ ) by comparison with the excitation energy of the X-rays ( $h\nu$ ), where  $E_k + E_b = h\nu$ , should give detailed information about the binding energy ( $E_b$ ) in various energy levels in the electron shell of an atom, thereby characterizing unambiguously every element. The binding energy of the electrons in different

states (core-levels), i.e. the internal energy level from which the electron is finally transferred to the “exterior”, is to be measured with respect to some well-defined reference level. As for free atoms and molecules the natural reference level is the vacuum level of the spectrometer, and for metals the most easily accessible reference level is the Fermi level, i.e. the binding energy is measured with respect to the binding energy of a Fermi-level electron with the metallic sample and the spectrometer being under electrical equilibrium. As for insulating samples the problem of the reference level is complicated by charging of the sample under X-ray irradiation and by the difficulty to localize the Fermi level within the energy band gap of the sample. There are methods that can be applied to cope with these difficulties and to get reliable binding energy data also for insulating samples referenced to the Fermi level of the spectrometer, and this reference can be scaled against known binding energies-to fix the zero point and the linearity of the energy scale. (For more details the interested reader may consult Ref. 1a, chapter 2.6, pp. 303-326 or Ref. 1b, chapter 1). In a first step we may then assume that the binding energy of a core-electron will be given by the equation  $E_b^{FL} = h\nu - E_k^{FL}$ , where  $h\nu$  is the photon energy and  $E_k^{FL}$  is the kinetic energy of the photoelectron measured with respect to the spectrometer Fermi level. However, there are numerous effects which can influence the energy of the outgoing electron, and in applying this equation we thereby seemingly experience changes of the energy level of the respective core electron by them.

It is well known that such core-level “shifts” of an atom result from so-called initial- and final-state effects [1a]. The relative contribution of the two effects is subtle and only partly experimentally accessible. According to Koopmans’ theorem we expect that the XPS spectra observed represent the electronic states of electrons in the atom before the photoemission process (initial state). The initial state effect (ISE) is first a static shift in the orbital energies in the ground state of the atom before core ionization due to a specific bonding situation of the atom, i.e. it has a direct relationship with the nature of the chemical bonds in which the atom is involved. But then the given electronic situation around the nucleus also affects the process of leaving of the electron induced by the impinging radiation. The number of electrons present and their kind of distribution in space will influence the shielding of the attractive force of the nucleus and thereby favour the ionization more or less. A change in the environment may modify the ground state valence charge of an atom and therefore the ability of the valence electrons to screen the final state hole.

As a final state effect (FSE) we may first consider the “response” of the electronic system of the atom to the creation of a core hole by relaxation processes. This will transfer additional energy to the outgoing electron and seemingly reduce the binding energy. Further analysis is complicated by final state effects related to the degree to which the extra-atomic environment can polarize in response to the ionization of the atom concerned. During the photo-ionization process such changes in the electronic environment due to the creation of the core-level vacancy also play a large role in influencing the measured binding energy. We imagine that such a polarization is essentially a movement of electron charge towards the core-ionized atom in the final state, and this again influences the ionization process.

Photoemission processes occur at time scales sufficiently slow to influence exiting electrons via attraction of the core-ionized atom (*adiabatic limit*), but there are also fast processes where the electron is emitted before the core-ionized atom relaxes (*sudden limit*). So, on the whole, for a correct interpretation of the measured values the perturbation of the electronic environment during the photoemission must be accounted for.

This paper will therefore begin with a more detailed description of initial- and final-state effects and of the diverse factors of influence. Such introductions into the topic have been given in literature before [1-5]. To keep a long story a little shorter we will therefore explain

some items in more detail in appendices to promote understanding. In this paper we venture to include new results from DFT calculations giving charges, electron densities and site potentials in such detailed interpretations. We hope to show how electron densities or charges of the atoms and potentials created by the surroundings play an important role as initial state effects, and we will also discuss how they contribute to specific final state effects. We venture to describe how properties of the ligands will influence the final state in a forthcoming paper.

## 2 Theory

### 2.1 Initial and final state contributions

The core-level binding energies are a most important fingerprint of the atoms in different environments. For an extensive discussion we refer to Ref. 1b (section 2). We present this survey on effects influencing XPS measurements of such binding energies by comparing the situation of an isolated atom in the gas phase with that of an atom embedded in chemical interactions in a solid. Fig.1 gives a schematic presentation of initial- and final-state effects for both cases in such a way as to show how the energy level of a core electron seemingly “moves” with respect to a chosen reference level by applying various corrections to eliminate different effects. (The height of the steps in the scheme is only qualitative in order to show the respective trend.) When “eliminating biases” produced by nucleus shielding, different electron densities, charges, site potentials etc. we should end up with the same energy of a specific core level in relation to our reference for both species, free atom and atom in the solid. As said before, the reference level for the gaseous species is the vacuum level and that for the solid is the Fermi level of the spectrometer, and this difference has also to be accounted for in the end.

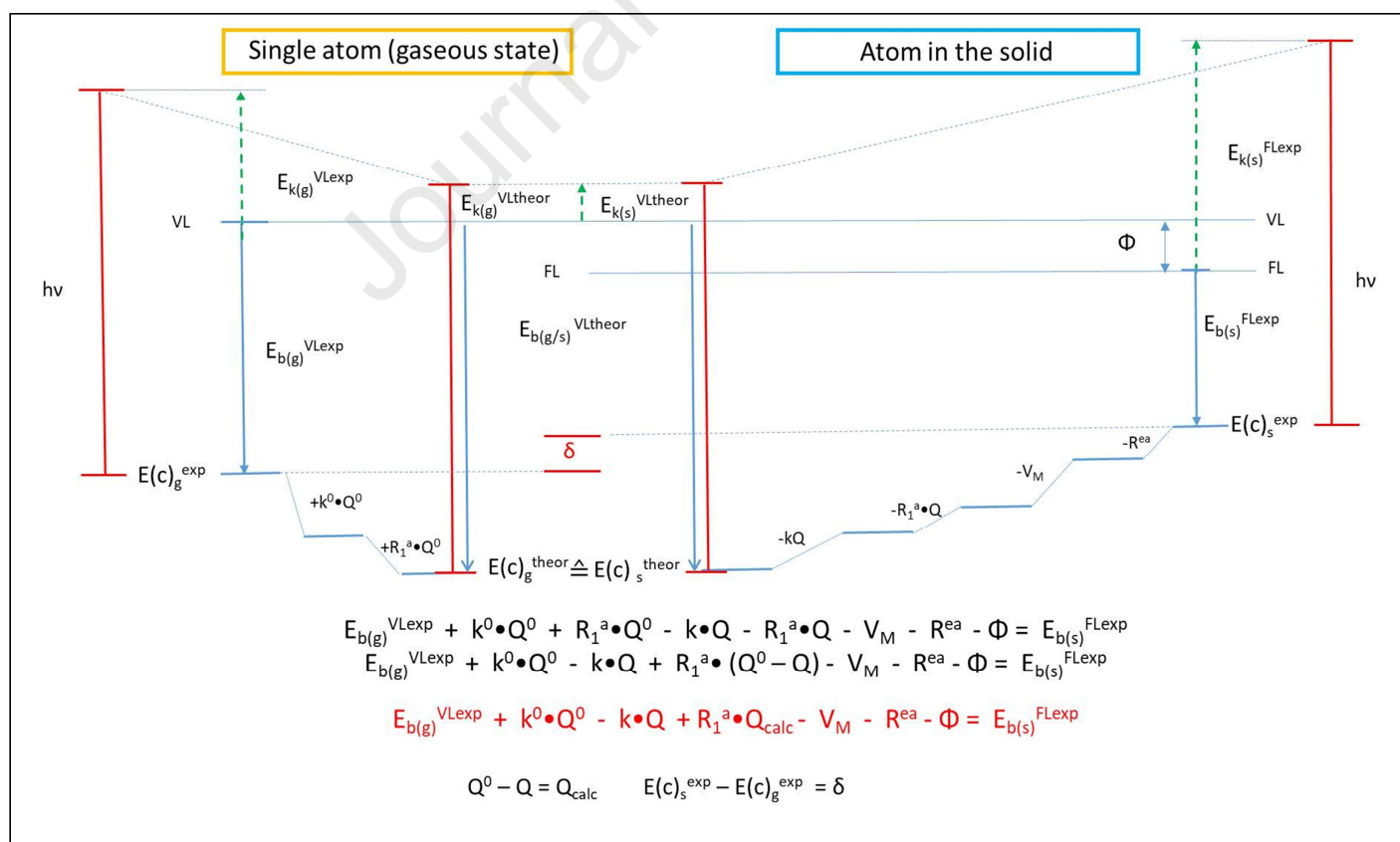


**Fig.1** A pictorial description of the contributions of initial and final state effects

Starting on the left side we describe the situation for the single atom. Given a certain excitation energy ( $h\nu$ ) the measured kinetic energy of the leaving electron can be converted to a binding energy  $E_{b(g)}^{VLexp} = h\nu - E_{k(g)}^{VLexp}$ . However, this value is “wrong” by the amount to which the other electrons around this nucleus have shielded its attracting charge and thereby increased the kinetic energy of the photoelectron and seemingly decreased the binding energy. Therefore, we must add a first correction term (named  $k^0Q^0$  for reasons described below) moving the energy level downwards and further away from our reference point. A second effect has also to be considered. The electronic system will subsequently relax when the core hole is produced, and the total energy change of the electronic system is added to the outgoing electron biasing our initial measurement in the same direction. So again we must add another term (named  $R_1^aQ^0$ , see below) to move the energy level downwards and give a higher binding energy. We have then arrived at the “true” energy of the core level  $E(c)_g^{theor}$  and could define a “true” theoretical binding energy by its distance from our reference and consequently also a theoretical kinetic energy of the exiting photon  $E_{k(g)}^{VLtheor}$ .

On the right side we start with the experimental result for the atom in a solid. We now measure in relation to the Fermi level, and - as said above - for the comparison with the single atom we have to relate this zero-level to the vacuum level used before by the so-called work function of the solid ( $\Phi$ ). Going to the left we see several steps downwards of which shielding effects by a different number of electrons compared to the single atom ( $kQ$ ) and consequently also a different relaxation energy ( $R_1^aQ$ ) are again part of the story. We now have to consider relaxation effects induced by the polarization of the surrounding atoms (named  $R^{ea}$ ) which again accelerate the outgoing electron and - last not least - the Madelung potential induced at the site of the atom by the whole collective of atoms in the crystal as a “helping hand” for the emission in the case of a cationic species (or a slowdown effect for anionic ones). (The graph in Fig. 1 gives the situation for a cationic species with a negative value for  $V_M$ .) The energy level ( $E(c)_s^{theor}$ ) which we now arrive at by all these “corrections” is the same as in the case of the free atom. We could calculate the experimental binding energy of an atom in the solid starting from the measured value for the free atom by moving in just these steps from left to right by first adding the different terms mentioned and then subtracting other terms again to go up all the steps reversely which bias the kinetic energy of the outgoing electron. The signs in this graph at the diverse steps refer to just this kind of process.

The difference  $\delta$  between the experimentally derived core level energies  $E(c)_g^{exp}$  and  $E(c)_s^{exp}$  represents the “chemical shift” of the atom embedded in the solid as compared to the free atom, and this is the information we are interested in when doing XPS.

To give it a concise mathematical description the general expression of the binding energy referenced to the Fermi level for the creation of a core hole left behind photoemission of the electron orbital  $c_i$  in a solid may be expressed as

$$E_{b(c_i)}^{FL}(\text{atom/solid}) = E_{b(c_i)}^{VL}(\text{free atom}) + k^0Q^0 - kQ + V_M - \Phi_{\text{solid}} - R(c_i) \quad (1a)$$

where  $E_{b(c_i)}^{VL}(\text{free atom})$  is the binding energy of the free atom referenced to the vacuum level [5].  $Q^0$  and  $Q$  are the valence charges (in units of number of electrons) of the free atom in the gas phase and of the atom in the solid sample under study,  $k^0Q^0$  (free atom) and  $kQ$  (atom/solid) represent the contribution of the valence electrons to the core-ionization energy with the factors  $k^0$  and  $k$  that depend on the inverse of the valence shell radius of the free atom and the atom in the solid, respectively, and which may be seen as shielding constants between the nucleus and the leaving electron by the valence electrons. A more detailed explanation for the terms “ $k^0Q^0 - kQ$ ” is given in a separate Appendix A in the Supplement.

There is an important connection between the parameters  $Q$  and  $k$ . A reduction of electron numbers due to electron transfer on bonding ( $Q^0 > Q$ ) also leads to a contraction of the electron cloud in the cationic species. Since  $k = 1/r$ , this means that  $k^0 < k$ . So, the two effects are in a way counteracting. This will be discussed in more detail in paragraph 5.2.

$V_M$  is the Madelung site energy (based on the charge  $Q_{\text{calc}}$  given by a different number of valence electrons as compared with the free atom ( $Q^0 - Q = Q_{\text{calc}}$ ), and  $\Phi_{\text{solid}}$  is the work function of the solid sample that must be added to have, to a good approximation, the binding energy referenced to the Fermi level of the solid sample which we assume to be in electrical equilibrium with the spectrometer. This term will be dealt with in an own section below (paragraph 5.4 and Appendix C in the Supplement). All these quantities described so far are related to the so-called initial state effects (ISE).

Since we focus on charges calculated by DFT ( $Q_{\text{calc}}$ ) and Madelung potentials based on just such charges, we may present Eq. (1a) also in a different form:

$$E_b(c_i)^{\text{FL}}(\text{atom/solid}) = E_b(c_i)^{\text{VL}}(\text{free atom}) + Q^0(k^0 - k) + kQ_{\text{calc}} + V_M - \Phi_{\text{solid}} - R(c_i) \quad (1b)$$

where the term  $V_M$  is negative for a cation or positive for an anion.

The last term in these equations represents the relaxation energy which is to be respected when trying to calculate  $E_b$  of the atom in the solid from the binding energy of the core level  $c_i$  in the free atom. In general relaxation energies contain an atomic and an extra-atomic part, so:  $R(c_i) = R^a(c_i) + R^{\text{ea}}(c_i)$ , and these contributions to the photoelectron process are described as final state effects (FSE).

Our equation describes the “movement” from the free atom to the one in the solid, as indicated in Fig.1, so the terms describing the relaxations should describe the “changes of relaxation during that movement”. The total relaxation contributions can be formulated as:

$$R_T(c_i) = R^a(c_i, \text{free atom}) + R(c_i) = R^a(c_i, \text{free atom}) + [R^a(Q) - R^a(Q^0)] + R^{\text{ea}}(c_i, \text{atom/solid}). \quad (1b')$$

The first part was “generated” by the relaxation of  $Q^0$  valence electrons and all the other core electrons. However, this first part must be omitted because we have already registered it as internal part of the measured  $E_b(c_i)^{\text{VL}}$ . So this leaves us with  $R(c_i)$  for the atom in the solid. We prefer to express such terms as product of the number of “acting” electrons times a relaxation per electron  $R_1^a$ . These terms can be calculated when considering the change of the number of “acting” electrons when going from the free atom to the one in the solid:

$$\begin{aligned} R(c_i) &= [R^a(Q) - R^a(Q^0)] + R^{\text{ea}}(\text{extra-atomic}) = -R_1^a \cdot (Q^0 - Q) + R^{\text{ea}}(\text{extra-atomic}) = \\ &= -R_1^a \cdot Q_{\text{calc}} + R^{\text{ea}}(\text{extra-atomic}), \end{aligned} \quad (1b'')$$

i.e. some of the atomic relaxation energy is lost for the cationic species because the valence electrons are  $Q$  and not  $Q^0$  as for the free atom. The full expression of equation (1a) will then be

$$\begin{aligned} E_b(c_i)^{\text{FL}}(\text{atom/solid}) &= \\ E_b(c_i)^{\text{VL}}(\text{free atom}) &+ k^0Q^0 - kQ + [V_M - \Phi_{\text{solid}}] + R_1^a \cdot Q_{\text{calc}} - R^{\text{ea}}(\text{extra-atomic}) \end{aligned} \quad (1c)$$

or

$$E_b(c_i)^{\text{FL}}(\text{atom/solid}) =$$

$$E_b(c_i)^{VL}(\text{free atom}) + Q^0(k^0 - k) + kQ_{\text{calc}} + [V_M - \Phi_{\text{solid}}] + R_1^a \cdot Q_{\text{calc}} - R^{\text{ea}}(\text{extra-atomic}) \quad (1d)$$

A similar discussion as the one given in Appendix A (see Supplement) for the meaning of  $k^0Q^0 - kQ$  leads us to understand the difference of atomic relaxation energies  $R^a$  depending on which core level is ionized. It is known that the relaxation energy is small for orbitals whose principal quantum number  $n$  is smaller than that of the orbital from which photoemission takes place. The relaxation energy is not very large either for orbitals where the principal quantum number  $n$  equals that of the orbital from which the electron is emitted. This too is a consequence of the Gauss-theorem applied to the shell structure of the atom. When a charge outside a concentric sphere containing electrons is changed this will not influence the field inside the sphere. An exact evaluation of these differences is extremely difficult. We therefore adhere to the simple definition of a mean relaxation effect per electron.

The Eqs.(1a and 1b) are a generalization and an extension of previous equations suggested by Broughton and Bagus [2a] and Fadley et al. [6]. In order to appreciate their approach we present it in a short form in Appendix A (in the Supplement).

In Appendix B (Supplement) we present the application of Eq.(1b) to specific cases that may be of interest: a free atom, a free ion and an atom in the metallic state.

In the next sections we will demonstrate how simple and effective the use of our Eq.(1c) can be. However, we have first to show how to calculate the final state effects,  $R(c_i)$ , by using the Auger parameter concept introduced by C.D. Wagner in 1972 [7]. It makes use of the experience that the kinetic energies of Auger electrons show even larger chemical shifts than the  $(c_i)$  core electron binding energies. The analytical utility of the X-ray excited Auger transitions was first pointed out by Wagner [7], Castle and Epler [8] and Shirley [9a].

## 2.2 Auger parameter

As mentioned before, the energies measured in the XPS experiment should be defined with respect to a known reference, i.e. vacuum or Fermi level, as shown in Fig.1. In the case of insulating and semiconductor-type solids a significant net positive charge accumulates on the surface and these “charging phenomena” make measurements difficult [1]. The C 1s binding energy (284.8 eV) from condensing background hydrocarbons onto a charged surface has been used for the Fermi level referencing of insulating and semiconducting samples. To cope with the charging phenomena C.D. Wagner defined a so-called Auger parameter  $\alpha$  [3, 7] which he defined as the difference between the kinetic energies of the photoelectron and the accompanying Auger electron. It is based on the fact that there is a fixed difference between two line energies (Auger and photoelectron) of the same element in the same sample, and that charge corrections to the individual peak measurements and work function corrections are unnecessary because they cancel during the calculation. Furthermore, vacuum level data can directly be compared to Fermi level data. Later he found it more useful to calculate a so-called modified Auger parameter  $\alpha'$  merging the binding energy of a core level with the kinetic energy of an associated Auger electron as given by the general equation

$$\alpha' = E_b^{\text{FL}}(c_1) + E_k^{\text{FL}}(c_1c_2c_3) = E_b^{\text{VL}}(c_1) + E_k^{\text{VL}}(c_1c_2c_3) \quad (2)$$

where  $c_1$  represents an electron core orbital of a given atom (free atom, atom/metal, atom/solid), and  $c_2$  and  $c_3$  are two core electrons of the same atom. (As for the cases where  $c_2$  and  $c_3$  may be a core electron and a valence electron, or two valence electrons, see comments in Ref. 3.) This relation of energies related to different reference levels may at first seem



surprising. It must be kept in mind that according to the definition of kinetic energies and binding energies the work function cancels out when forming these sums. So, the kinetic energy of the Auger ( $c_1c_2c_3$ ) electron and the binding energy of a core electron of the atom under study, recorded in the same spectrum, are added together to obtain a quantity that does *not depend on the reference level* (the vacuum or the Fermi level) and, in the case of insulating or semiconductor-type solids, *not on any charging phenomena* either.

A schematic presentation of the processes involved in a photoemission of a ( $c_1$ ) core-electron and in the Auger ( $c_1c_2c_3$ ) process is shown in Fig.2.

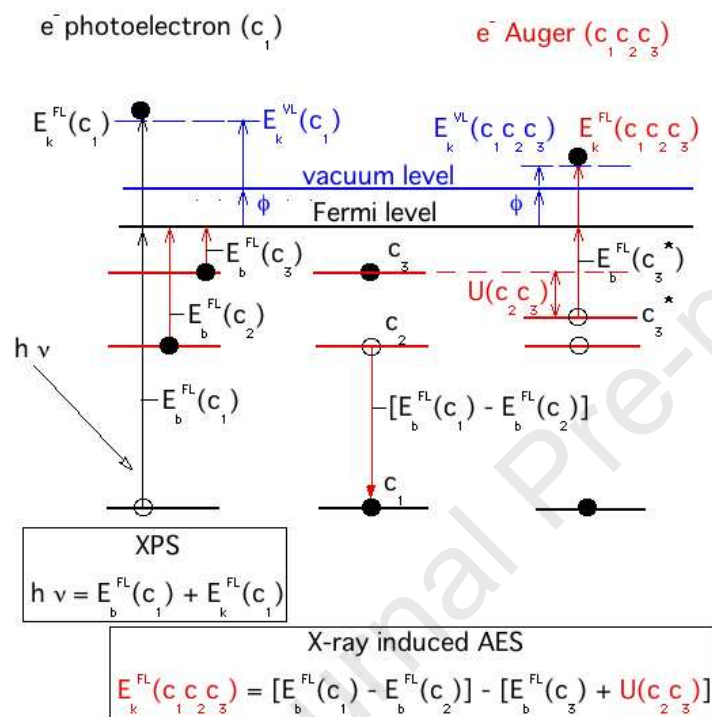


**Fig.2** Schematic presentation of kinetic and binding energies involved in the photoemission of a ( $c_1$ ) core-electron and in the Auger ( $c_1c_2c_3$ ) process

The kinetic energy of Auger electrons itself gives additional information on the chemical state of an atom. Wagner [7], Castle and Epler [8], and Shirley [9a] were the first authors who pointed out the analytical utility of the X-ray excited Auger transitions in XPS, having observed for several elements in different chemical states larger chemical shifts for the ( $c_1c_2c_3$ ) Auger electron kinetic energy with respect to the chemical shift of the ( $c_1$ ) core electron binding energy. The combination of  $E_b^{FL}(c_1)$  and  $E_k^{FL}(c_1c_2c_3)$  is therefore even more valuable.

For present purposes we shall apply Eq.(2) to Ba, Pb, Zn and Cu compounds in which the outer orbitals  $c_2$  and  $c_3$  are the same (see Supplement).

The kinetic energy of the Auger transition may be written as

$$E_k^{FL}(c_1c_2c_3) = E_b^{FL}(c_1) - E_b^{FL}(c_2) - E_b^{FL}(c_3) - U(c_2c_3) \quad (3a)$$

where  $U(c_2c_3)$  represents the effective repulsion energy between the  $c_2$  and  $c_3$  holes in the

final-state of the Auger process (see Fig.2). This quantity may be written to a good approximation as [3, 5]

$$U(c_2c_3) = R_T(c_2) + R_T(c_3) - R_T(c_2c_3) + F^a(c_2c_3) \quad (3b)$$

The term  $F^a(c_2c_3)$  represents the LSJ-dependent bare repulsion energy between the  $c_2$  and  $c_3$  electrons (holes), depending only on the atom and not on its chemical state.

For the free atom the kinetic energy of the Auger transition and the effective repulsion energy between the  $c_2$  and  $c_3$  holes in the final state may be written as

$$E_k^{VL}(c_1c_2c_3)_{\text{free atom}} = E_b^{VL}(c_1)_{\text{free atom}} - E_b^{VL}(c_2)_{\text{free atom}} - E_b^{VL}(c_3)_{\text{free atom}} - U(c_2c_3)_{\text{free atom}} \quad (3c)$$

and

$$U(c_2c_3)_{\text{free atom}} = R^a(c_2, \text{free atom}) + R^a(c_3, \text{free atom}) - R^a(c_2c_3, \text{free atom}) + F^a(c_2c_3) \quad (3d)$$

The Auger parameters for the atom in the solid under study, and for the free atom, according to Eq.(2) can be written as

$$\alpha'(\text{atom/solid}) = E_k^{FL}(c_1c_2c_3) + E_b^{FL}(c_1) = [E_b^{FL}(c_1) - E_b^{FL}(c_2)] + [E_b^{FL}(c_1) - E_b^{FL}(c_3)] - U(c_2c_3) \quad (4a)$$

and

$$\alpha'(\text{free atom}) = E_k^{VL}(c_1c_2c_3)_{\text{free atom}} + E_b^{VL}(c_1)_{\text{free atom}} = [E_b^{VL}(c_1)_{\text{free atom}} - E_b^{VL}(c_2)_{\text{free atom}}] + [E_b^{VL}(c_1)_{\text{free atom}} - E_b^{VL}(c_3)_{\text{free atom}}] - U(c_2c_3)_{\text{free atom}} \quad (4b)$$

The difference between the binding energies of two deep core levels of the atom in two different chemical states is, to a good approximation, an atomic constant, i.e. the two levels have the same chemical shift that is independent from the chemical state [3]. Therefore assuming  $[E_b^{FL}(c_1) - E_b^{FL}(c_2)] = [E_b^{VL}(c_1)_{\text{free atom}} - E_b^{VL}(c_2)_{\text{free atom}}]$ , and  $[E_b^{FL}(c_1) - E_b^{FL}(c_3)] = [E_b^{VL}(c_1)_{\text{free atom}} - E_b^{VL}(c_3)_{\text{free atom}}]$  we can write

$$\alpha'(\text{atom/solid}) - \alpha'(\text{free atom}) = -U(c_2c_3) + U(c_2c_3)_{\text{free atom}} \quad (5a)$$

Considering the Eqs. (3b and 3d) we may write the Auger parameter shift as

$$\alpha'(\text{atom/solid}) - \alpha'(\text{free atom}) = -R_T(c_2) - R_T(c_3) + R_T(c_2c_3) + R^a(c_2, \text{free atom}) + R^a(c_3, \text{free atom}) - R^a(c_2c_3, \text{free atom}) \quad (5b)$$

that according to the equation  $R_T(c_i) = R^a(c_i, \text{free atom}) + R(c_i)$  becomes

$$\alpha'(\text{atom/solid}) - \alpha'(\text{free atom}) = -R(c_2) - R(c_3) + R_T(c_2c_3) - R^a(c_2c_3, \text{free atom}) \quad (5c)$$

Considering  $R(c_i) = [R^a(Q) - R^a(Q^0)] + R^{ea}(\text{extra-atomic}) = -R_1^a \cdot (Q^0 - Q) + R^{ea}(\text{extra-atomic})$  we see that  $R(c_2) = R(c_3) = R(c_1) = -R_1^a \cdot (Q^0 - Q) + R^{ea}(\text{extra-atomic})$ .

It is also evident that within the approximations discussed above the total relaxation energies are related to each other by the following relations

$$R_T(c_1) = R_T(c_2) + A_1(c_1c_2)$$

$$R_T(c_1) = R_T(c_3) + A_1(c_1c_3)$$

$$R_T(c_2) = R_T(c_3) + A_1(c_2c_3) \quad (5e)$$

where  $A_1(c_1c_2)$ ,  $A_1(c_1c_3)$  and  $A_1(c_2c_3)$  are atomic constants independent of the chemical state.

The relaxation energies are dominated by classical Coulomb interaction so that we can assume that

$$R_T(c_2c_3) = 4 R_T(c_2) + A_2(c_2c_3) \quad (5f)$$

$$R^a(c_2c_3, \text{ free atom}) = 4 R^a(c_2, \text{ free atom}) + A_2(c_2c_3) \quad (5g)$$

where  $A_2(c_2c_3)$  is an atomic constant independent of the chemical state.

The Auger parameter shift becomes

$$\alpha'(\text{atom/solid}) - \alpha'(\text{free atom}) = 2 R(c_1) \quad (6)$$

Finally, Eq.(6) shows that differences in the relaxation (or polarization) energy, which is a valuable piece of chemical information, can be obtained experimentally by using the Auger parameter shift between the two chemical states.

### 2.3 Wagner plot

The kinetic energy of the  $(c_1c_2c_3; {}^{2S+1}L_J)$  Auger electron, the binding energy of the  $(c_1)$  core electron, and the Auger parameter  $(c_1, c_1c_2c_3; {}^{2S+1}L_J)$  can be displayed in a diagram called the Wagner plot (WP), which is of considerable analytical utility. Such a kind of plot was first proposed by Wagner in 1979 [7], and such plots are widespread since [3-5]. Note that in this plot the abscissa,  $E_b^{FL}(c_1)$ , is oriented in the negative direction. (Under the approximations used to derive Eq.(6), it is evident that the Auger parameter for the atom under study could be calculated by adding the kinetic energy of the most intense and sharp  $(c_1c_2c_3)$  Auger transition to the binding energy of a chosen  $c_1$  core level,  $E_b^{FL}(c_1)$ , depending on what is the most suitable core level accessible with the available X-ray source.)

In case the relation  $[E_b^{FL}(c_1) - E_b^{FL}(c_2)] = \text{const}$  is not valid, as in case of P and S containing compounds - where the 2p core levels of S and P are spatially modified by alteration of the atomic environment and can only be considered *core-like* and not true core-type as the 1s electrons - a different approach is necessary to link the Auger parameter shift with the relaxation energy, as discussed in Ref. 3 and by Hohlneicher et al.[10].

The natural reference chemical state is, of course, the free atom state. To put the free atom data in the Wagner plot for the atom in solid compounds we move the free atom binding energy of the core electron and the kinetic energy of the Auger electron from the vacuum level to the Fermi level of the bulk metal according to Eq.(1a), considering  $k = k^0$ ,  $Q = Q^0$ ,  $V_M = 0$ , and  $R = 0$  :

$$E_b(c_1)^{FL}(\text{free atom}) = E_b(c_1)^{VL}(\text{free atom}) - \Phi_{\text{metal}} \quad (7a)$$

$$E_k^{FL}(c_1c_2c_3) (\text{free atom}) = E_k^{VL}(c_1c_2c_3) (\text{free atom}) + \Phi_{\text{metal}} \quad (7b)$$

The following equations describe the rationale behind the Wagner plot and show how it can be used to estimate initial- and final-state effects.

By using Eqs. (1b) and (6) [3-5] it is possible to demonstrate that

$$E_k^{\text{FL}}(c_1c_2c_3) = I' - 3E_b^{\text{FL}}(c_1) \quad (8)$$

where the quantity  $I'$ , called the *initial state parameter*, is given by the equation

$$I'(\text{atom/solid}) = \alpha'(\text{free atom}) + 2[E_b^{\text{VL}}(\text{free atom}) + Q^0(k^0 - k) + kQ_{\text{calc}} + V_M - \Phi_{\text{solid}}] \quad (9a)$$

The initial state effect is due to the static situation of the system, i.e. the energy levels of the electron states in question before the excitation process which are influenced by internal mutual interaction of core and valence electrons on the one hand and by external effects such as charge formation and external potentials by chemical bonding on the other hand.

Eq.(8) shows that a set of compounds, with similar initial-state effects at the core-ionized site, may be described in a Wagner plot by a straight line with a slope of -3 though, on account of the aforementioned inversion of the abscissa, it looks like a line having a slope of +3.

The intercept of the straight line of Eq.(8) with the ordinate, calculated for a given chemical state as  $I' = E_k^{\text{FL}}(c_1c_2c_3) + 3E_b^{\text{FL}}(c_0)$ , is given by the sum of two quantities separated out of Eq.(9a):  $\{\alpha'(\text{free atom}) + 2[E_b^{\text{VL}}(\text{free atom}) + k^0Q^0]\}$ , which depends only on properties of the free atom, and  $2[-kQ^0 + kQ_{\text{calc}} + V_M - \Phi_{\text{solid}}]$ , which depends only on the initial-state properties of the core-ionized atom in the solid under study.

An experimental confirmation of the relation  $R(c_2c_3) \approx 4R$  (and of  $R = R(c_2) = R(c_3) = R(c_1)$ ) can be found in the Wagner plots of several elements drawn using the NIST database [11]. A common finding is that a class of compounds with similar initial-state contributions present Auger kinetic-energy shifts three times larger in size, and of opposite sign, compared to the binding energy shifts (see the WP for Ba, Pb, Zn and Cu compounds shown in Fig.4).

The initial-state parameter of the free atom, *referenced to the Fermi level*, is obtained from Eq.(9a) considering that  $Q = Q^0$ ,  $k^0 = k$ ,  $V_M = 0$ , and  $\Phi_{\text{solid}} = \Phi_{\text{metal}}$

$$I'(\text{free atom}) = \alpha'(\text{free atom}) + 2E_b^{\text{VL}}(\text{free atom}) - 2\Phi_{\text{metal}} \quad (9b)$$

The initial-state parameter shift of the atom in the solid compound with respect to the initial-state parameter of the free atom is

$$\Delta I' = 2[(k^0Q^0 + \Phi_{\text{metal}}) + kQ_{\text{calc}} - kQ^0 + V_M - \Phi_{\text{solid}}] \quad (10)$$

It is important to note that in a Wagner plot a set of compounds with the same relaxation energy (constant Auger-parameter values, see Eq.(6)) will be shown, according to Eq.(2), on a common line with a slope of -1, (again, apparently with a slope of +1).

According to Eqs.(1b) and (6) the Auger-parameter shift (i.e. the final-state shift) with respect to the free atom is

$$\Delta\alpha' = 2R = -2Q_{\text{calc}} \cdot R_1^a + 2R^{\text{ea}}(\text{extra-atomic}) \quad (11)$$

The two quantities on the right side may be calculated using quantum-chemical and electrostatic models, and the results are found in good agreement with Auger parameter shifts [12, 13].

(In previous work [12] an application of an electrostatic model for estimating Auger parameter shifts in an analysis of the local environment was presented. It could be shown that the calculated shifts ( $\Delta\alpha'$ ) are a function of the number, local geometry and electronic

polarizability of nearest-neighbour atoms of the core-ionized one. This model describes the final-state polarization process at the core-ionized atom by a classical electrostatic calculation involving the total electric field “felt” by the ligands, i.e., the one generated by the central positive charge plus the one due to the induced dipole on the ligands in the first coordination shell. We will not go into further details here.)

### 3 Preview

We give a first résumé. As noticed above it will be difficult to extract values for several of the different terms in all these equations from XPS measurements. The definition of the Auger parameter and especially the use of Wagner plots allow us to separate initial and final state effects and to extract at least possible ranges of variation of binding energies and Auger energies influenced by them.

Quantum chemical calculations give a possibility to estimate energy levels and their differences, and a comparison with measured binding energies may be helpful, at least on a relative scale. The work presented here focusses on the application of results of DFT calculations to quantify several of the terms in Eq.(1a) more accurately, and this pertains especially to the electron densities or charges ( $Q^0$  and  $Q$ ) and the dimensions of electron clouds (as addressed in the  $k^0$  and  $k$  values). There is a strong debate whether DFT calculations are appropriate to calculate XPS spectra [2b]. We must emphasize that our approach is not to be compared with other results described in literature where DFT methods were used to define energies of electron core levels. They have been used successfully to study core-level spectroscopies and, especially, to determine the main XPS peaks of organic molecules. However, DFT is inherently a one electron configuration theory, and more complicated multiplets and multi-configurations are not easy to handle with such methods. We repeat that this is not the scope of our investigations. We only use DFT to estimate some of the parameters needed for the solution of our equation.

Furthermore, we present values for Madelung site potentials resulting from the specific structures of compounds and the charges calculated from a Bader analysis of the electron densities. Thorough studies on the effect of Madelung energies on binding energies have been published before [14, 15], however, the authors have used formal oxidation states as charges for their calculations, and, consequently, they deplore many inconsistencies of their approach. It will be shown here that charges resulting from the Bader analysis of the electron distributions give far better consistencies with the variations of binding energies by Madelung effects. The subtle interaction of the different terms contributing to initial state effects can well be demonstrated by dint of such parameters. As a set of compounds for such a demonstration we have chosen the mono-chalcogenides and the di-halides of the main group element Ba and of Zn as representatives of closed shell configurations and of Pb because of its special electron configurations as  $ns^2$  element. Additionally, we have included compounds of the monovalent transition element Cu and then also compounds of divalent Cu as open shell representatives to show how specific electron configurations modify the general picture.

### 4 Experimental

All calculations within the Density Functional Theory formalism were performed using the VASP 5.2 package [16, 17] together with the projector-augmented-wave (PAW) method of Blöchl [18] and the GGA functional as proposed by Perdew, Burke and Enzerhof (PBE) [19]. In some cases we have also repeated the calculations using GW functionals as supplied with the VASP package to estimate the possible variations.

A cutoff of 550 eV for the expansion of the plane-waves basis set was defined, and the integration in the Brillouin zone was done over a  $\Gamma$ -centred mesh of equally spaced k-points within the irreducible part of the Brillouin zone using the Tetrahedron method with Blöchl corrections [20]. Convergence of the total energy in the calculated structures with the number of k-points has been checked. Atoms were allowed to relax to a residual force  $< 0.01$  eV/Å. The subsequent Bader analysis was performed on a previously calculated charge density grid using the Bader Charge Analysis Code [21, 22].

The same code also gives the volumes of the electron basins, a value which we have used to define a radius of the respective electron clouds which is needed for the k values in Eq.(1a) by approximating the volumes by a spherical form. The sum of the radii thereby calculated will eventually exceed typical atomic distances resulting from the fact that electron density is not spherically distributed and may in part bulge outside the interatomic connection vector. We feel that such k values nevertheless give a good estimate.

The onsite-potentials were calculated using the Ewald-Bertaut method as implemented in the programme COUPOT [23]. The transition parameter defining the split between calculations in direct or reciprocal space was optimized so as to have an equal number of terms in both parts. Variations on further changing this procedure did not result in changes  $> 0.001$  eV.

When discussing the relation between the  $V_M$  and the kQ terms in Eq.(1a) in the following paragraphs we show how the topology of the different structures influences this relation, and we introduce a so-called “geometric factor” GF characterizing the different crystal structures of our compounds generally given by  $GF = V_M/q$ , q being the formal charge of the ion. We instead use the charge  $Q_{\text{calc}} = (Q^0 - Q)$  as calculated by DFT (see Eq.(1d) to calculate  $V_M$  and then also to define this factor as  $GF = V_M/Q_{\text{calc}}$ . The relation of GF to the usual terms used in the discussion of Madelung energies may be given as follows.

The total Madelung factor (MF) of a structure is the sum of Partial Madelung factors (PMF) describing the contribution of the individual ions on different crystallographic sites,  $MF = \sum PMF$ . A “reduced” Partial Madelung factor is defined as  $PMF^* = PMF / Q_{\text{calc}}^2$ , and correspondingly a “reduced total Madelung factor” is given by  $MF^* = \sum PMF^*$ . It is common practice to relate these values to the shortest interatomic distance R. The relation between the local Madelung energy  $V_M$  and PMF is given by

$$PMF = -(R/2) \cdot Q_{\text{calc}} \cdot V_M \text{ or } (PMF/R) \cdot (2/ Q_{\text{calc}}) = -V_M = GF \cdot Q_{\text{calc}}. \quad (12a)$$

Since  $PMF / Q_{\text{calc}}^2$  is  $PMF^*$ , we can write

$$(2/R) \cdot PMF^* = - GF. \quad (12b)$$

So, this geometric factor GF is a kind of short-hand notation of the topology of a structure scaled to the shortest interatomic distance and unit charges.

The binding energies and the Auger energies used in this paper have been chosen from literature and from the NIST data base [11] as documented in the tables reported in the Supplement. Table 1 presents all calculated data used in the following discussions.

**Table 1** List of compounds and related data (Note that in the fifth column we report the product kQ with  $Q = Q^0 - Q_{\text{calc}}$ .)

| Compound            | Cation charge $Q_{\text{calc}}$ | Cation volume ( $\text{\AA}^3$ ) | $k = 14.4/r$ (eV) (r in $\text{\AA}$ ) | kQ (eV) | Madelung energy term at the cationic site (eV) | Geometric factor GF (eV) | Binding energy $E_b$ (eV) | Auger kinetic energy (eV) | Auger parameter $\alpha'$ (eV) | $\Delta\alpha'$ (eV) | WF (eV) |
|---------------------|---------------------------------|----------------------------------|--|---------|--|--------------------------|---------------------------|---------------------------|--------------------------------|----------------------|---------|
| Zn <sub>g</sub>     |                                 |                                  | 10.12                                  |         |  |                          | 1028.9                    | 974.4                     | 2003.3                         | 0                    |         |
| Zn <sub>s</sub>     |                                 |                                  | 9.73                                   |         |  |                          | 1021.7                    | 992.1                     | 2013.8                         | 10.5                 | 4.45    |
| ZnO-w               | 1.2                             | 10.31                            | 10.67                                  | 8.53    | -14.35   | -11.96                   | 1022.1                    | 987.7                     | 2009.8                         | 6.5                  | 5.79    |
| ZnO-s               | 1.16                            | 10.62                            | 10.56                                  | 8.87    | -13.65   | -11.77                   | 1022.1                    | 987.7                     | 2009.8                         | 6.5                  | 5.79    |
| ZnS-w               | 0.81                            | 13.24                            | 9.81                                   | 11.67   | -8.18  | -10.23                   | 1021.6                    | 989.7                     | 2011.3                         | 8                    | 5.26    |
| ZnS-s               | 0.80                            | 13.45                            | 9.76                                   | 11.71   | -8.06  | -9.95                    | 1021.8                    | 989.7                     | 2011.3                         | 8                    | 5.26    |
| ZnSe-w              | 0.67                            | 14.97                            | 9.42                                   | 12.53   | -6.5   | -9.7                     | 1022.0                    | 989.5                     | 2011.5                         | 8.2                  | 5.12    |
| ZnSe-s              | 0.65                            | 15.11                            | 9.39                                   | 12.68   | -6.34  | -9.75                    | 1022.0                    | 989.5                     | 2011.5                         | 8.2                  | 5.12    |
| ZnTe                | 0.43                            | 17.3                             | 8.98                                   | 14.1    | -3.85  | -8.95                    | 1021.6                    | 991.3                     | 2012.9                         | 9.6                  | 4.94    |
| ZnF <sub>2</sub> -r | 1.46                            | 8.15                             | 11.53                                  | 6.23    | -15.78   | -10.81                   | 1021.8                    | 986.2                     | 2008                           | 4.7                  | 7.84    |
| ZnF <sub>2</sub> -a | 1.43                            | 7.98                             | 11.62                                  | 6.62    | -15.25   | -10.66                   | 1021.8                    | 986.2                     | 2008                           | 4.7                  | 7.84    |
| ZnCl <sub>2</sub>   | 1.03                            | 12.66                            | 9.96                                   | 9.66    | -7.71  | -7.49                    | 1023.7                    | 986.2                     | 2009.9                         | 6.6                  | 6.74    |
| ZnBr <sub>2</sub>   | 0.86                            | 14.01                            | 9.63                                   | 10.98   | -6.44  | -7.49                    | 1023.4                    | 987.3                     | 2010.7                         | 7.4                  | 6.35    |
| ZnI <sub>2</sub>    | 0.64                            | 16.01                            | 9.21                                   | 12.53   | -4.53  | -7.08                    | 1022.5                    | 988.7                     | 2011.2                         | 7.9                  | 5.88    |
|                     |                                 |                                  |  |         |  |                          |                           |                           |                                |                      |         |
| Ba <sub>g</sub>     |                                 |                                  | 5.83                                   |         |  |                          | 788.7                     | 576.8                     | 1365.5                         | 0                    |         |
| Ba <sub>s</sub>     |                                 |                                  | 5.84                                   |         |  |                          | 780.6                     | 601.0                     | 1381.6                         | 16.1                 | 2.68    |
| BaO                 | 1.48                            | 25.13                            | 7.93                                   | 4.1     | -13.36   | -9.03                    | 779.4                     | 597.8                     | 1377.2                         | 11.7                 | 4.49    |
| BaS                 | 1.42                            | 28.91                            | 7.56                                   | 4.38    | -11.19   | -7.88                    | 779.3                     | 599.2                     | 1378.5                         | 13.0                 | 4.08    |
| BaSe                | 1.36                            | 30.14                            | 7.46                                   | 4.77    | -10.38   | -7.63                    | -                         | -                         | -                              |                      | 3.97    |
| BaTe                | 1.34                            | 31.72                            | 7.33                                   | 4.84    | -9.63  | -7.19                    | -                         | -                         | -                              |                      | 3.83    |
| BaF <sub>2</sub>    | 1.68                            | 25.50                            | 7.89                                   | 2.52    | -14.72   | -8.76                    | 780.0                     | 595.8                     | 1375.8                         | 10.3                 | 6.62    |
| BaCl <sub>2</sub>   | 1.6                             | 26.94                            | 7.74                                   | 3.09    | -11.92   | -7.45                    | 780.4                     | 596.5                     | 1376.9                         | 11.4                 | 5.69    |
| BaBr <sub>2</sub>   | 1.55                            | 27.54                            | 7.69                                   | 3.46    | -11.03   | -7.12                    | -                         | -                         | -                              | -                    | 5.36    |
| BaI <sub>2</sub>    | 1.49                            | 30.18                            | 7.46                                   | 3.80    | -9.86  | -6.62                    | -                         | -                         | -                              | -                    | 4.96    |
|                     |                                 |                                  |  |         |  |                          |                           |                           |                                |                      |         |
| Pb <sub>g</sub>     |                                 |                                  | 8.18                                   |         |  |                          | 144.3                     | 81.3                      | 225.6                          | 0                    |         |
| Pb <sub>s</sub>     |                                 |                                  | 7.3                                    |         |  |                          | 136.7                     | 96.3                      | 233.0                          | 7.4                  | 3.89    |
| PbO-t               | 1.15                            | 29.66                            | 7.5                                    | 6.38    | -11.85   | -10.22                   | 137.7                     | 92.6                      | 230.3                          | 4.5                  | 5.42    |
| PbS                 | 1.02                            | 25.11                            | 7.93                                   | 7.77    | -8.61  | -8.44                    | 137.5                     | 94.6                      | 232.05                         | 6.45                 | 6.5     |
| PbSe                | 0.81                            | 27.84                            | 7.66                                   | 9.12    | -6.65  | -8.21                    | 137.6                     | 94.8                      | 232.35                         | 6.8                  | 4.79    |
| PbTe                | 0.63                            | 29.88                            | 7.48                                   | 10.25   | -4.87  | -7.73                    | 137.25                    | 95.5                      | 232.7                          | 7.1                  | 4.62    |
| PbF <sub>2</sub>    | 1.56                            | 22.45                            | 8.23                                   | 3.62    | -14.4  | -9.12                    | 138.5                     | 90.6                      | 229.1                          | 3.5                  | 7.5     |
| PbCl <sub>2</sub>   | 1.3                             | 24.90                            | 7.95                                   | 5.55    | -9.97  | -7.67                    | 138.9                     | 92.1                      | 231.0                          | 5.4                  | 6.44    |
| PbBr <sub>2</sub>   | 1.16                            | 27.21                            | 7.72                                   | 6.48    | -8.65  | -4.79                    | 138.8                     | 92.6                      | 231.4                          | 5.8                  | 6.07    |
| PbI <sub>2</sub>    | 0.93                            | 28.67                            | 7.58                                   | 8.11    | -5.53  | -5.95                    | 138.35                    | 93.4                      | 231.7                          | 6.1                  | 5.62    |
|                     |                                 |                                  |  |         |  |                          |                           |                           |                                |                      |         |
| Cu <sub>g</sub>     |                                 |                                  | 13.4                                   |         |  |                          | 939.7                     | 900.7                     | 1840.4                         | 0                    |         |
| Cu <sub>s</sub>     |                                 |                                  | 10.18                                  |         |  |                          | 932.63                    | 918.6                     | 1851.2                         | 10.8                 | 4.48    |
| Cu <sub>2</sub> O   | 0.52                            | 14.48                            | 9.52                                   | 4.57    | -6.637   | -12.76                   | 932.18                    | 917.0                     | 1849.2                         | 8.8                  | 5.33    |
| Cu <sub>2</sub> S * | 0.38                            | 13.17                            | 9.83                                   | 6.09    | -3.93  | -10.02                   | 932.62                    | 917.2                     | 1849.8                         | 9.4                  | 5       |

|  |       |        |       |       |         |        |        |       |        |      |      |
|--|-------|--------|-------|-------|---------|--------|--------|-------|--------|------|------|
| Cu <sub>2</sub> Se *                                   | 0.26* | 13.03* | 9.87* | 7.30* | -1.91*  | -7.34* | 932.5  | 917.8 | 1850.3 | 9.9  | 4.91 |
| Cu <sub>2</sub> Te                                     | 0.11  | 15.56  | 9.30  | 8.28  | -0.835  | -7.59  | -      | -     | -      | -    | 4.79 |
| CuCl   | 0.58  | 15.45  | 9.35  | 3.91  | -5.813  | -10.02 | 932.34 | 915.2 | 1847.5 | 7.1  | 6.09 |
| CuBr   | 0.46  | 16.74  | 9.07  | 4.90  | -4.431  | -9.63  | 932.27 | 915.7 | 1848.0 | 7.6  | 5.83 |
| CuI  | 0.3   | 17.94  | 8.87  | 6.21  | -2.654  | -8.85  | 932.5  | 916.3 | 1848.8 | 8.4  | 5.5  |
| CuFeS <sub>2</sub>                                     | 0.55  | 13.35  | 9.79  | 4.40  | -5.963  | -10.84 | 932.14 | 918.0 | 1850.2 | 9.8  | 5.14 |
| CuO  | 0.96  | 11.02  | 10.43 | 10.85 | -11.595 | -12.08 | 933.76 | 917.6 | 1851.3 | 10.9 | 5.81 |
| CuS-1  | 0.46  | 14.46  | 9.53  | 14.68 | -5      | -10.86 | 932.2  | 918.1 | 1850.3 | 9.9  | 5.28 |
| CuS-2  | 0.51  | 13.69  | 9.70  | 14.5  | -4.97   | -9.74  | 932.2  | 918.1 | 1850.3 | 9.9  | 5.28 |
| CuSe-h-1   | 0.33  | 16.46  | 9.13  | 15.25 | -3.613  | -10.95 | 932.0  | 918.4 | 1850.4 | 10.0 | 5.14 |
| CuSe-h-2   | 0.38  | 15.44  | 9.32  | 15.10 | -3.527  | -9.28  | 932.0  | 918.4 | 1850.4 | 10.0 | 5.14 |
| CuSe-r-1   | 0.33  | 15.73  | 9.27  | 15.48 | -3.734  | -11.32 | 932.0  | 918.4 | 1850.4 | 10.0 | 5.14 |
| CuSe-r-2   | 0.39  | 15.33  | 9.35  | 15.5  | -3.561  | -9.13  | 932.0  | 918.4 | 1850.4 | 10.0 | 5.14 |
| CuTe   | 0.13  | 13.66  | 9.71  | 18.16 | -0.380  | -2.92  | -      | -     | -      | -    | 4.96 |
| CuF <sub>2</sub>                                       | 1.29  | 9.76   | 10.86 | 7.71  | -14.024 | -10.87 | 936.38 | 915.4 | 1851.7 | 11.3 | 7.86 |
| CuCl <sub>2</sub>                                      | 0.84  | 13.84  | 9.67  | 11.22 | -6.755  | -8.04  | 935.3  | 915.1 | 1850.4 | 10.0 | 6.75 |
| CuBr <sub>2</sub>                                      | 0.66  | 15.19  | 9.37  | 12.56 | -4.905  | -7.43  | 934.5  | 916.1 | 1850.6 | 10.2 | 6.37 |
| Cu(OH) <sub>2</sub>                                    | 1.19  | 10.51  | 10.60 | 8.58  | -13.815 | -11.61 | 934.67 | 916.3 | 1850.9 | 10.5 | 6.66 |
| CuSO <sub>4</sub>                                      | 1.18  | 10.38  | 10.64 | 8.72  | -13.09  | -11.09 | 936.0  | 915.9 | 1851.9 | 11.5 | 6.69 |
| Cu <sub>3</sub> (PO <sub>4</sub> ) <sub>2</sub> -<br>1 | 1.13  | 11.76  | 10.21 | 8.88  | -14.616 | -12.93 | 935.85 | 915.8 | 1851.6 | 11.2 | 6.39 |
| Cu <sub>3</sub> (PO <sub>4</sub> ) <sub>2</sub> -<br>2 | 1.11  | 11.83  | 10.19 | 9.07  | -15.307 | -13.79 | 935.85 | 915.8 | 1851.6 | 11.2 | 6.39 |
| Cu(NO <sub>3</sub> ) <sub>2</sub>                      | 1.12  | 11.18  | 10.38 | 9.13  | -10.083 | -9     | 935.51 | 915.0 | 1850.5 | 10.1 | 7.05 |

w wurtzite-type s sphalerite-type r rutile-type a  $\alpha$ -PbO<sub>2</sub>-type

h hexagonal-type r orthorhombic-type

-1 or -2 different sites in the same structure

\* arithmetic mean of many different sites in the same structure

- not available or modification unclear

## 5 Discussion

The influence of bonding type has long been discussed in XPS studies, (see e.g. Ref.1b Chapter 3.1). All approaches consider the charges of the atoms or - more generally speaking - the degree of ionicity as an important factor, and this is verified in the following plot (Fig.3) where we show how measured binding energies in the form of Auger parameters and cation charges calculated by DFT correlate on a  $\Delta$ EN scale using Pauling's electronegativity values for the Zn compounds under study. To demonstrate the "accuracy" of Auger parameters we give mean values and variations for the Zn Auger parameters found in literature for the respective Zn compounds. (We have assembled XPS data from literature for all compounds discussed in this paper in a Supplement to show how the values may vary depending on measuring conditions. We have also selected data from this list which we believe to be more reliable for our investigations.) Furthermore, the plot shows how little calculated Bader charges change on using different potentials in the DFT calculations (GGA and GW). The influence of charge as the result of  $\Delta$ EN on the Auger parameters is clearly seen, however, the correlation is not univariate or linear.



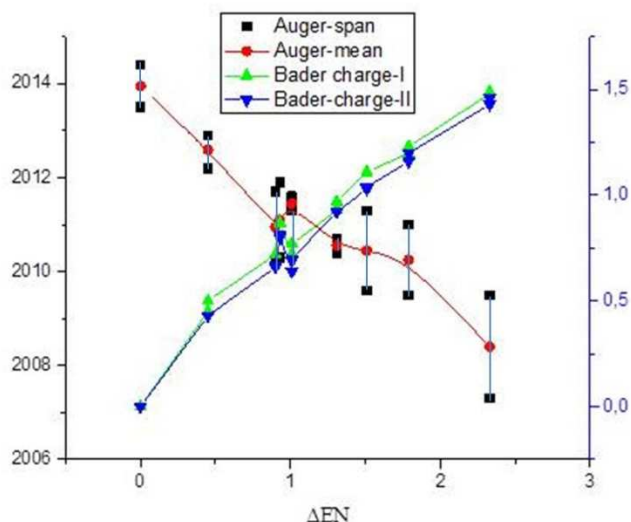


**Fig. 3** Auger parameters and Bader charges plotted vs. electronegativity differences for Zn compounds. Triangles give calculated charges of the Zn cations for GW and GGA potentials, circles give mean Auger parameters, squares describe the spread of data in literature. The right scale gives the Bader charges and the left one the Auger parameters in eV (see text).

In the following paragraphs we will therefore examine Wagner plots of Ba, Zn, Pb and Cu compounds and then analyse initial and final-state effects in more detail in view of the results of our DFT calculations. It will become evident how the outcome of such calculations contributes to a deeper understanding of the measured values of binding energies.

### 5.1 A first overview by Wagner plots

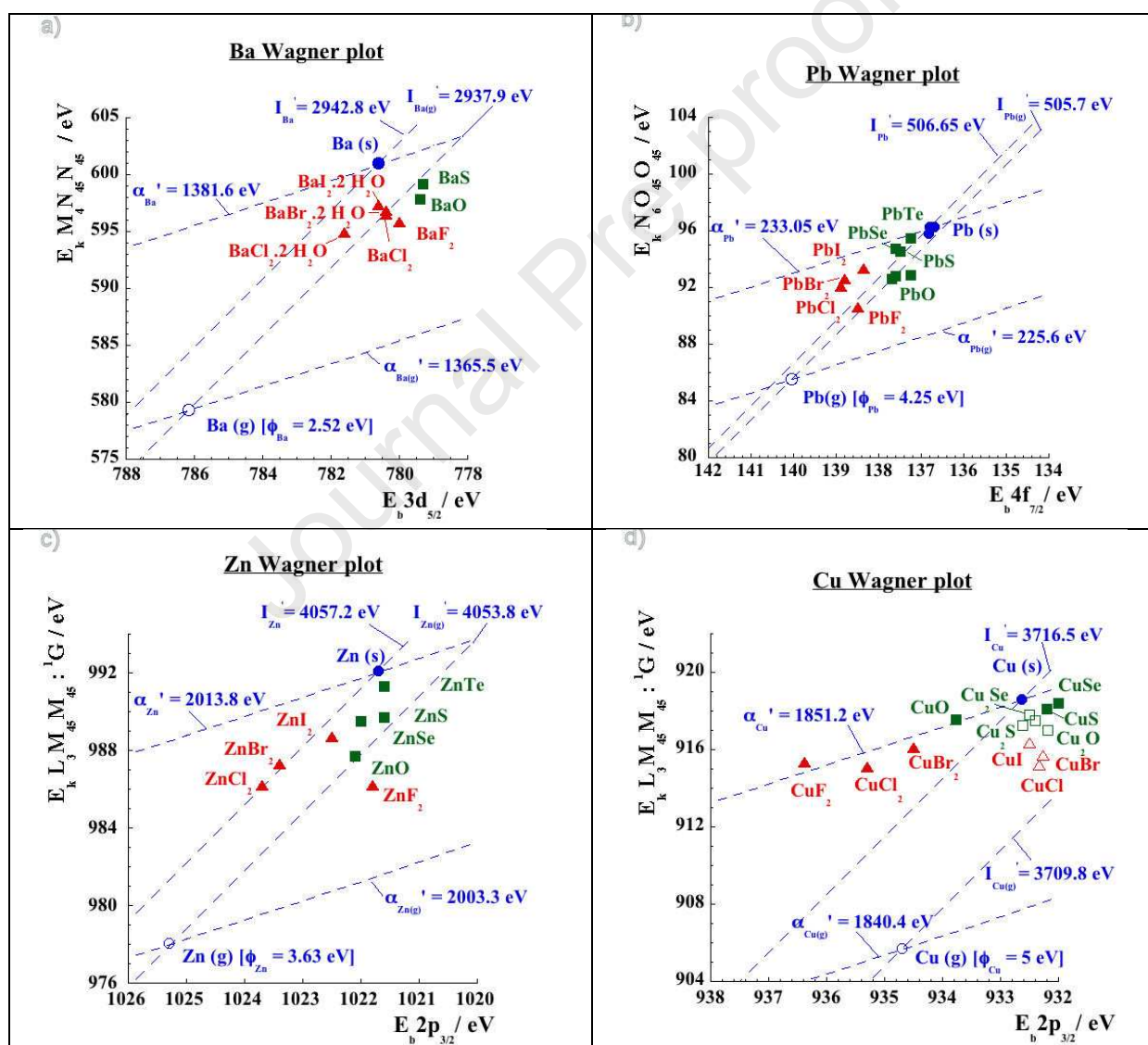
The plots in Fig.4 (a-e) give an overview of the measured XPS data in the form of Wagner plots for Ba, Zn, Pb and Cu compounds. (The data for Cu have been expanded to other than chalcogenides and halides in order to demonstrate the striking difference between Cu(I) and Cu(II) compounds.) All data on the  $E_b^{\text{FL}}(c_0)$  core-electron binding energy, the Auger electron  $E_k^{\text{FL}}(c_1c_2c_3)$  kinetic energy and the Auger parameter  $\alpha' = E_k^{\text{FL}}(c_1c_2c_3) + E_b^{\text{FL}}(c_0)$  are reported in the Supplement (note that the  $c_0/c_1$  core levels are  $3d_{5/2}/3d_{3/2}$  for Ba,  $4f_{7/2}/4f_{5/2}$  for Pb, and  $2p_{3/2}/2p_{3/2}$  for both Zn and Cu). The dashed reference lines with slope +1 give the orientation of constant Auger parameters ranging from the value for the free atom ( $\alpha'_{(\text{Ba,Zn,Pb,Cu})g}$ ) to the one for the element in the respective solid ( $\alpha'_{(\text{Ba,Zn,Pb,Cu})s}$ ), and the other set with slope +3 should unite compounds with similar initial state effects.

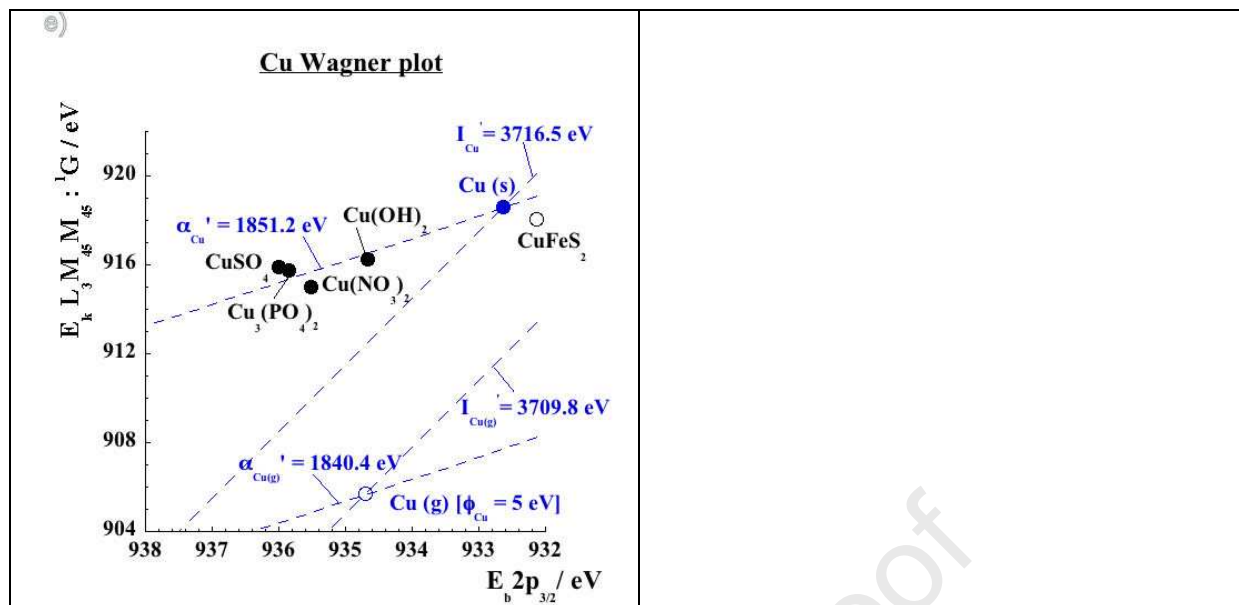
As said before, we see that the sequence of abscissa values, i.e. the relation of binding energies of an element in different compounds, will not meet our expectations with respect to bonding type and charges. The scatter is quite irregular. However, this parameter is at least appropriate to classify chalcogenides and halides in different groups, the former all having lower binding energies of the respective core levels. It is also interesting to see that different structural modifications of a compound may result in different positions of the respective ticks, i.e. *the structure of the atomic environment influences the binding energy*.

The situation is a little better when we move a parallel to the two  $\alpha'$  lines from the one giving the free atom data to the other for the metal. We cross the values for the different compounds in a sequence which is similar to the sequence of electronegativity differences but only on an ordinal scale. However, there are still some inconsistencies.

A similar scan across the diagrams with a line with slope +3 gives quite different results for the three series of compounds. The ticks even spread outside the range given by the values for the free atom and the elemental metal. We may see a weak tendency of all ticks aligned along a line with this slope. But the scatter is quite strong. The halides of Zn and Pb can be grouped as having similar initial state effects, but here the fluorides are out of the line. This tells us that the various contributions to the initial and final states add up quite differently in these compounds. We will therefore study the different terms given in Eq.(1a) in more detail.

**Fig.4** Wagner plots for a) Ba, b) Pb, c) Zn, d and e) Cu. All data used to draw the plots are reported in the Supplement.





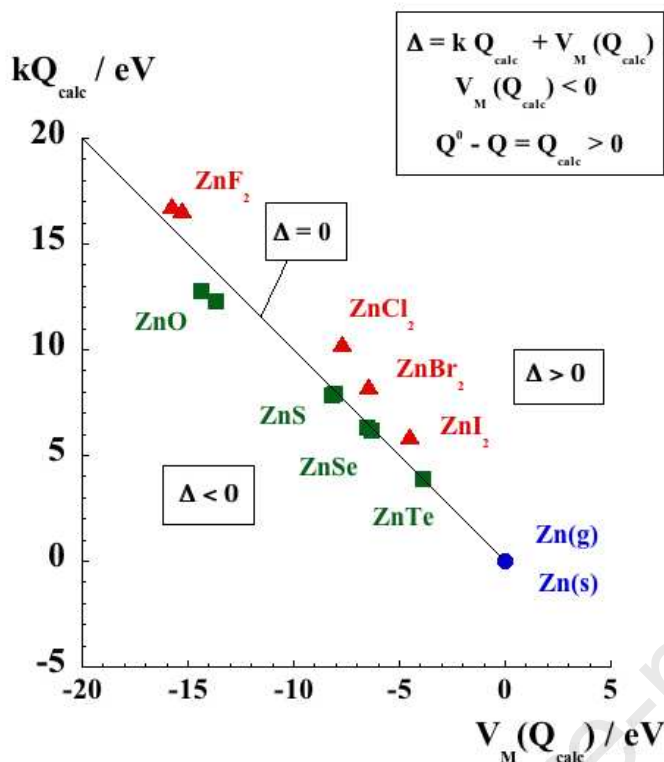
## 5.2 Initial state effects

As stated above the contribution to the initial state effects is given by the quantity  $[Q^0(k^0-k) + kQ_{\text{calc}} + V_M - \Phi_{\text{solid}}]$  which within the framework of our simple model may be calculated according to Eq.(1b) and Eq.(6)

$$E_b(c_i)^{\text{FL}}(\text{atom/solid}) - E_b(c_i)^{\text{VL}}(\text{free atom}) + \Delta\alpha' / 2 = Q^0(k^0-k) + kQ_{\text{calc}} + V_M - \Phi_{\text{solid}} \quad (13)$$

As said before, the term  $Q^0(k^0-k)$  gives a correction term for the effect of the change from the total electron set of the free atom to that of the atom in the solid which has led to a change of the binding energy, and the last term is a correction factor to transfer the energies from the vacuum level to the Fermi level of the solid. This leaves us with two terms representing the situation in the solid,  $kQ_{\text{calc}}$  and  $V_M(Q_{\text{calc}})$ , i.e. the valence charge density of the atom in the solid and the local Madelung site potential induced by the total surrounding structure of the solid which will then either help or hinder the outgoing photoelectron to leave a cationic or an anionic species respectively. The balance of these two terms and the question which of the two outbalances the other one is decisive for the kinetic energy of the outgoing electron.




Surprisingly, these two parameters have quite similar values and they compensate each other more or less. We describe their relation in the different compounds by the sum  $\Delta = kQ_{\text{calc}} + V_M(Q_{\text{calc}})$  (which is essentially a difference in the case of cations because  $V_M$  is a negative quantity at a cationic site). Fig.5 summarises these compensatory effects for the Zn compounds under study as an example.



**Fig.5** The balance of  $kQ_{\text{calc}}$  vs.  $V_M(Q_{\text{calc}})$  for Zn compounds

The situation  $\Delta = 0$  is depicted by the straight line in this diagram. The  $kQ_{\text{calc}}$  term overrides the potential term for most of the halides ( $\Delta > 0$ ). Both terms are quite balanced for most of the chalcogenides.  $\text{ZnF}_2$  lies only slightly in the  $\Delta > 0$  field. In plots for the other elements under study (not shown here) here we see some stronger deviations from the  $\Delta = 0$  line.  $\text{PbO}$  is a very special case insofar as this compound is distinctly “out of balance” and we find that some  $\text{Cu(II)}$  compounds have mostly moved into the  $\Delta < 0$  field, and this merits an own discussion as given below. These “misfits” give clear evidence that a specific electron configuration and *the respective structures of the compounds play a decisive role*.

Crystal chemical discussions focus very much on size relations of atoms and ions. The typical tetrahedral coordination in most of the Zn compounds and the high coordination numbers for the Ba and Pb compounds are an outcome of such relations. Together with the particular charges of the ions the respective topology of the structures governed by such size relations leads to a specific potential at an ion site ( $V_M/e$ ). DFT calculations provide another set of sizes, i.e. the volume of the electron clouds, which we use in this approach to define a radius for the calculation of  $k$  values. As said above, these sizes may not be congruent with the typical ionic radii as documented in tables (e.g. Shannon et al. [24]) since the electron distribution in basins will not be exactly spherical in the different structures. Fig.6 gives some examples for the size and form of electron basins of cations in different coordination environments, the geometric form of a basin always being the dual form of the respective coordination polyhedron.

|   |   |   |
|---|---|---|
|  |  |  |
| coordination number 4<br>(tetrahedral)  | coordination number 6<br>(octahedral)   | Coordination number 7   |

**Fig.6** Electron basins of cations within typical coordination spheres as examples

The “competition” between  $kQ_{\text{calc}}$  and  $V_M$  comes down to a comparison between a local topology of electron density and a potential built up from a collective arrangement of charge points. It is surprising to see how they match in part and how they deviate in some cases. To emphasize the effect of topology we have chosen to eliminate the charge effect and to contrast  $k$  values with a so-called geometric factor (GF) involving the structural information in a distinct form. GF is calculated by dividing the potential at the ion site by the charge (see Experimental, Eq.(12b)). So, the diagrams in Fig.7 are in a sense a magnified view of such ones like Fig.5 showing in more detail the influence of the geometry of the structures on the deviations from the  $kQ_{\text{calc}}/V_M$  balance  $\Delta = 0$  which is marked as dotted lines. The other lines should give help to the eye to group halides and chalcogenides.

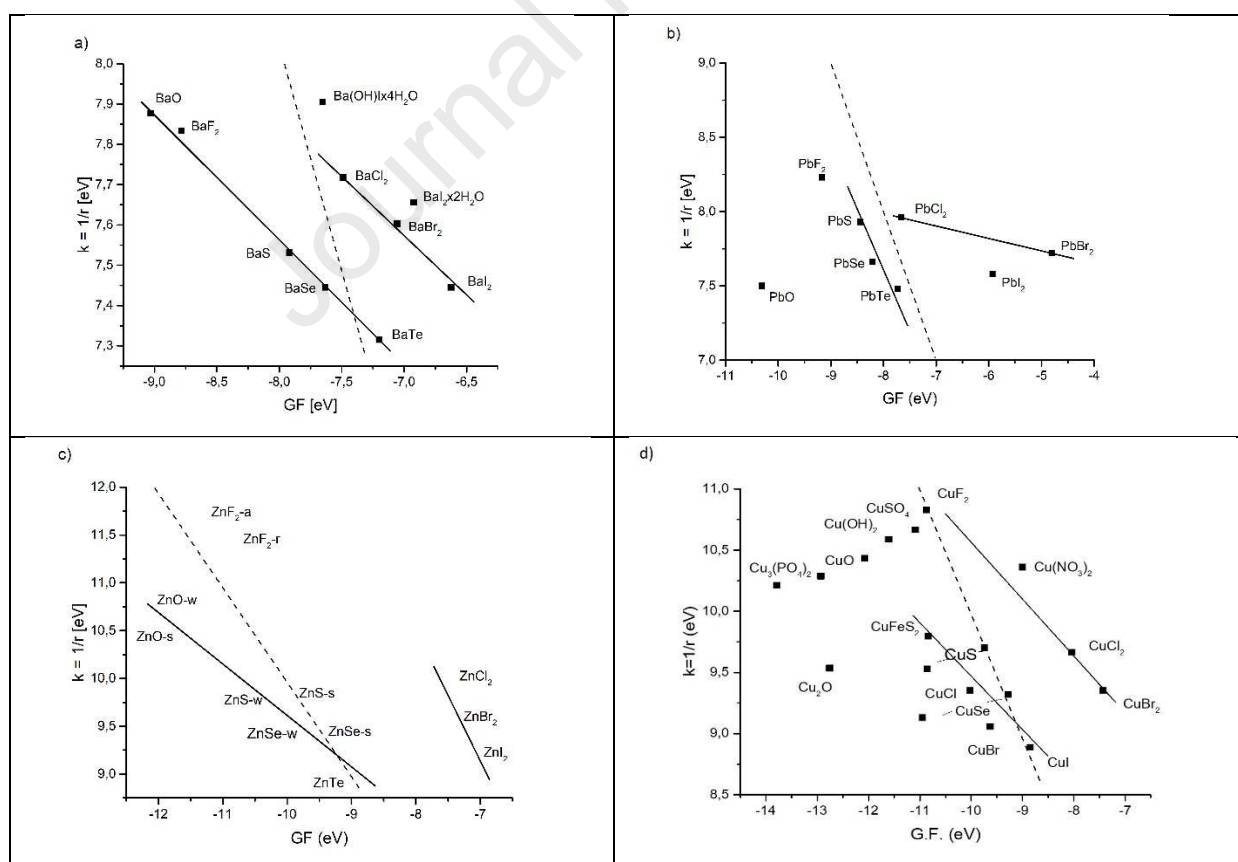


**Fig.7** A comparison of  $k$  values ( $k = 14.4/r$  in eV,  $r$  in Å) and geometric factors (GF) for the a) Ba, b) Pb, c) Zn and d) Cu compounds

For an interpretation we must keep in mind that the charges – and consequently also the potentials – will grow with the electronegativity differences ( $\Delta EN$ ) of the elements in a compound, and with growing charges the electron clouds of the cations will contract, i.e.  $1/r$  will increase. With increasing  $\Delta EN$  we should move along a negative diagonal upwards in these diagrams, and this is generally the case in all series.

The Ba chalcogenides – all having a rocksalt type structure with six-fold coordination of the cation - are well assembled on a line mostly in the  $\Delta < 0$  field. The potential dominates less when going from the oxide to the telluride, i.e. reduced potential values and larger interatomic distances “improve” the  $k/GF$  balance. For the halides - all having the same  $PbCl_2$ -type structure with 7+2 coordination of the cation - the ticks move closer to the  $\Delta = 0$  line in the opposite potential/distance relation.  $BaF_2$  has a fluorite-type structure with eightfold coordination of Ba, and it is far on the other side of the  $\Delta = 0$  line. This structure type has a large Madelung-factor, and consequently the local potential is large.

The chalcogenides of Zn and Pb show the same trend. They move closer to the  $\Delta = 0$  line with reduced potentials and larger interatomic distances. The electron configuration of Pb is inert in these cases. The isostructural chloride and bromide of Pb behave like the respective isostructural Ba compounds. However, the Pb halides move faster to the left with increasing ionicity which nevertheless does not lead to the respective contraction of the electron clouds in these cases, evidently due to the lone pair configuration. Pb iodide with a different structure and a different Madelung-factor is out of this line. The heavier halides of Zn with fourfold cation coordination stay well out of balance in the  $\Delta > 0$  field. The Zn-fluoride modifications with coordination number 6 are quite different. The rutile structure is a “more favourable” geometric arrangement with a larger Madelung-factor, so these ticks move to the left and closer to the  $\Delta = 0$  line.

$PbO$  behaves quite differently. The lone pair activity of Pb is clearly mapped in this diagram. The large potential and a large geometric factor are contrasted by a “seemingly huge” electron cloud. In the Wagner plot given in Fig.4b we find the  $PbO$  tick at a smaller binding energy compared to the other compounds, perhaps similar only to  $PbTe$ . The binding energy is much lower than expected. The  $k$  values of these compounds representing the size of the electron clouds are quite similar also. However, in the latter compound the  $ns^2$  electron pair is rather inert, whereas in  $PbO$  it is a lone pair with large excentricity. The general trend as given by  $\Delta EN$  is out of order in the case of  $PbO$ , and this inconsistency might tempt us to speculate that the non-spherical electron distribution in the cloud is responsible for it. This peculiarity will be dealt with in another context in the final “conclusion” section.

The diagram giving the  $1/r$  vs.  $GF$  relation for the Cu compounds seems to be quite different at first sight. This is because it contains other compounds than halides and chalcogenides and that not all chalcogenides have been included because their XPS data are not available. Furthermore, we note that the ticks of compounds with different formal oxidation numbers are separated in this field. The more ionic Cu(II) compounds are assembled in the upper part of the diagram. The dihalides follow a common trend moving closer to the  $\Delta = 0$  line with increasing ionicity like the other cations discussed above. The Cu(I) halides, on the contrary, move away from the equilibrium line with increasing cationic charge. They behave surprisingly like the chalcogenides of Ba, Pb and Zn. The general difference between Cu(I) and Cu(II) compounds will also be an important item in the following paragraphs dealing with final state effects and in our “Conclusion”.

To summarize we can state that the delicate balance between  $kQ_{calc}$  and  $V_M$  is an important contribution to the initial state effects. The seemingly surprising scatter of the various ticks in Wagner plots may well be rationalized considering the results of such DFT and Madelung-

type calculations. It becomes evident that *not only the local electron density but also the topology of the solid structures plays a decisive role.*

To finish up this paragraph we focus once more on the graph for Ba compounds in Fig.7. XPS data for non-hydrated Ba-halides are not available, evidently because they are deliquescent compounds and difficult to handle. To show the effect of water in the first coordination sphere we have also included ticks calculated for a known hydrate of the di-iodide and of a hydroxy-iodide. The ticks of the water containing compounds are well off the line for the Ba halides and much higher than for BaI<sub>2</sub>, itself, just as one would expect due to the higher charges induced by a larger mean  $\Delta EN$ , and with a higher charge the electron cloud is more contracted changing the initial state contribution. Furthermore, the coordination sphere is now different. The coordination number is 7 (BaI<sub>7</sub>) in BaI<sub>2</sub>, 8 (BaI(H<sub>2</sub>O)<sub>6</sub>OH) in BaI(OH)•4H<sub>2</sub>O and finally even 9 (BaI<sub>5</sub>(H<sub>2</sub>O)<sub>4</sub>) in BaI<sub>2</sub>•2H<sub>2</sub>O. The change in ligands and the increase of ligand distances will now also influence the R term in our fundamental equation, i.e. the final state effect. So, the hydration will have considerable effect both on the initial state terms  $kQ_{\text{calc}}$  and  $V_M$  and on the final state term and thereby on measured XPS data. This will often be the cause for differing XPS data of hygroscopic materials.

### 5.3 Final state effects: atomic and extra-atomic contributions

The last term in Eqs.(1a and b), R, calculated according to Eq.(11), describes the relaxation of the electronic system after the excitation by the impinging radiation:

$$\Delta\alpha'/2 = R = - Q_{\text{calc}} \cdot R_1^a + R^{\text{ea}}(\text{extra-atomic}) \quad (14)$$

$- Q_{\text{calc}} \cdot R_1^a$  represents the modification of the atomic relaxation energy due to the valence charge difference between the atom under study and the free atom.  $R^{\text{ea}}$  is the contribution arising from the relaxation of electrons of neighbour atoms (extra-atomic). To a first approximation for the atom in the solid compound under study we assume that  $R_1^a$  (free atom) represents the atomic relaxation energy *per* valence electron. This quantity may be estimated from the nonrelativistic numerical Hartree-Fock calculations of core electron binding energies for free atoms and ions reported by Broughton and Bagus [2a] to obtain atom-ion core level shifts for use in analyzing XPS data. The unrelaxed (Koopmans' theorem) Eigenvalue and the relaxed ( $\Delta$ SCF) core-ionization energies are calculated by nonrelativistic self-consistent Hartree-Fock programs.

The difference between the Eigenvalue and the  $\Delta$ SCF value represents the atomic relaxation energy:

$$\Delta\text{SCF} = \text{Eigenvalue} - R^a \quad (15a)$$

Considering Eq.(1a) applied to a free ion, it is possible to write

$$\Delta\Delta\text{SCF} = E_b(c_i)^{\text{VL}}(\text{free ion}) - E_b(c_i)^{\text{VL}}(\text{free atom}) = \Delta\text{Eigenvalue} - \Delta R^a \quad (15b)$$

$$\Delta\text{Eigenvalue} = k^0 Q^0 - kQ \quad (15c)$$

$$\Delta R^a = [R^a(Q) - R^a(Q^0)] = - Q_{\text{calc}} \cdot R_1^a \quad (15d)$$

where  $R_1^a$  represents *the atomic relaxation energy per valence electron.*

Therefore

$$\Delta\Delta\text{SCF} = k^0 Q^0 - kQ + Q_{\text{calc}} R_1^a \quad (15e)$$

The results of these calculations on Ba(g), Pb(g), Zn(g) and Cu(g) free atoms, and on Ba<sup>2+</sup>(g), Pb<sup>2+</sup>(g), Zn<sup>2+</sup>(g) and Cu<sup>+</sup>/Cu<sup>2+</sup>(g) free ions are reported in Table 2. In this table we also report the values of  $k^0$  in eV and of the atomic radius  $r_0$  in Å ( $k^0 = 14.4/r_0$ ).

**Table 2** Relaxation energy per valence electron,  $R_1^a$ (free atom), for Zn a), Pb b), Ba c) and Cu d) free atoms calculated from the relaxation energies reported by Broughton and Bagus [2a]. In the table we also report the  $k^0$  values (eV) for the free atoms calculated according to Eqs.(15a-15e). The atomic radius  $r_0$  (in Å) is estimated by the relation  $k^0 = 14.4/r_0$ .

**a) Zn free atom and Zn<sup>2+</sup> free ion with a 2p core hole:**

| Free atom and ion                           | $\Delta\text{SCF}$<br>(eV) | Eigenvalue<br>(eV) | $R^a$<br>(eV) | $R_1^a$ (eV)        | $k$ (eV)<br>(*) | $r$ (Å)<br>(*) |
|---|----------------------------|--------------------|---------------|---------------------|-----------------|----------------|
| Zn (3d <sup>10</sup> 4s <sup>2</sup> )      | 1031.605                   | 1059.223           | 27.618        |                     | 10.12           | 1.42           |
| Zn <sup>2+</sup> (3d <sup>10</sup> )        | 1054.099                   | 1079.462           | 25.363        |                     |                 |                |
| $\Delta\Delta\text{SCF}$                    | 22.494                     |                    |               |                     |                 |                |
| $\Delta R^a$                                |                            |                    | 2.255         | $R_{1(s)}^a = 1.13$ |                 |                |
| $Q = Q_s = 0$                               |                            |                    |               |                     |                 |                |
| $Q_{\text{calc}} = Q_{\text{calc}(s)} = +2$ |                            |                    |               |                     |                 |                |

$$(*) \Delta\Delta\text{SCF} = k^0 Q^0 - kQ + Q_{\text{calc}(s)} R_{1(s)}^a$$

$$\Delta\Delta\text{SCF}(\text{Zn}^{2+} - \text{Zn}) = 22.494 = k_{\text{Zn}}^0 \times 2 + 2R_{1(s)}^a, \text{ then } k_{\text{Zn}}^0 = 10.12 \text{ eV and } r_{\text{Zn}0} = 1.42 \text{ \AA}.$$

**b) Pb free atom and Pb<sup>2+</sup> free ion with a 4f core hole:**

| Free atom and ion                           | $\Delta\text{SCF}$<br>(eV) | Eigenvalue<br>(eV) | $R^a$<br>(eV) | $R_1^a$ (eV)         | $k$ (eV)<br>(*) | $r$ (Å)<br>(*) |
|---|----------------------------|--------------------|---------------|----------------------|-----------------|----------------|
| Pb (6s <sup>2</sup> 6p <sup>2</sup> )       | 165.660                    | 179.120            | 13.462        |                      | 8.177           | 1.76           |
| Pb <sup>2+</sup> (6s <sup>2</sup> )         | 183.550                    | 195.476            | 11.926        |                      |                 |                |
| $\Delta\Delta\text{SCF}$                    | 17.890                     |                    |               |                      |                 |                |
| $\Delta R^a$                                |                            |                    | 1.536         | $R_{1(p)}^a = 0.768$ |                 |                |
| $Q = Q_p = 0$                               |                            |                    |               |                      |                 |                |
| $Q_{\text{calc}} = Q_{\text{calc}(p)} = +2$ |                            |                    |               |                      |                 |                |

$$(*) \Delta\Delta\text{SCF} = k^0 Q^0 - kQ + Q_{\text{calc}(p)} R_{1(p)}^a$$

$$\Delta\Delta\text{SCF}(\text{Pb}^{2+} - \text{Pb}) = 17.890 = k_{\text{Pb}}^0 \times 2 + 2R_{1(p)}^a, \text{ then } k_{\text{Pb}}^0 = 8.177 \text{ eV and } r_{\text{Pb}0} = 1.76 \text{ \AA}.$$



**c) Ba free atom and Ba<sup>2+</sup> free ion with a 3d core hole:**

| Free atom and ion                             | $\Delta$ SCF (eV) | Eigenvalue (eV) | R <sup>a</sup> (eV) | R <sub>1</sub> <sup>a</sup> (eV)       | k (eV) (*) | r (Å) (*) |
|---|-------------------|-----------------|---------------------|--|------------|-----------|
| Ba(6s <sup>2</sup> )                          | 808.757           | 827.306         | 18.549              |  | 5.833      | 2.47      |
| Ba <sup>2+</sup> [Xe]                         | 821.798           | 838.971         | 17.173              |  |            |           |
| $\Delta\Delta$ SCF                            | 13.041            |                 |                     |  |            |           |
| $\Delta$ R <sup>a</sup>                       |                   |                 | 1.376               | R <sub>1(s)</sub> <sup>a</sup> = 0.688 |            |           |
| Q = Q <sub>s</sub> = 0                        |                   |                 |                     |  |            |           |
| Q <sub>calc</sub> = Q <sub>calc(s)</sub> = +2 |                   |                 |                     |  |            |           |

$$(*)\Delta\Delta\text{SCF} = k^0Q^0 - kQ + Q_{\text{calc(s)}}R_{1(s)}^a$$

$$\Delta\Delta\text{SCF}(\text{Ba}^{2+} - \text{Ba}) = 13.041 = k_{\text{Ba}}^0 \times 2 + 2R_{1(s)}^a, \text{ then } k_{\text{Ba}}^0 = 5.833 \text{ eV and } r_{\text{Ba}^0} = 2.47 \text{ \AA}.$$

**d) Cu free atom and Cu<sup>+</sup> and Cu<sup>2+</sup> free ions with a 2p core hole:**

| Free atom and ions  | $\Delta$ SCF (eV) | Eigenvalue (eV) | R <sup>a</sup> (eV) | R <sub>1</sub> <sup>a</sup> (eV)      | k (eV) (eV) (*) | r (Å) (*) |
|---|-------------------|-----------------|---------------------|---------------------------------------|-----------------|-----------|
| Cu (3d <sup>10</sup> 4s <sup>1</sup> )                              | 941.514           | 969.235         | 27.721              |                                       | 13.4            | 1.07      |
| Cu <sup>+</sup> (3d <sup>10</sup> )                                 | 951.265           | 977.693         | 26.428              |                                       | 18.3            | 0.787     |
| $\Delta\Delta$ SCF  | 9.751             |                 |                     |                                       |                 |           |
| $\Delta$ R <sup>a</sup>   |                   |                 | 1.293               | R <sub>1(s)</sub> <sup>a</sup> = 1.29 |                 |           |
| Q=Q <sub>s</sub> +Q <sub>d</sub> = 0 + 1                            |                   |                 |                     |                                       |                 |           |
| Q <sub>calc</sub> = Q <sub>calc(s)</sub> = +1                       |                   |                 |                     |                                       |                 |           |
| Cu <sup>2+</sup> (3d <sup>9</sup> )                                 | 972.028           | 996.052         | 24.024              |                                       |                 |           |
| $\Delta\Delta$ SCF  | 30.514            |                 |                     |                                       |                 |           |
| $\Delta$ R <sup>a</sup>   |                   |                 | 2.404               | R <sub>1(d)</sub> <sup>a</sup> = 2.40 |                 |           |
| Q = Q <sub>s</sub> +Q <sub>d</sub> = 0 + 0                          |                   |                 |                     |                                       |                 |           |
| Q <sub>calc</sub> = Q <sub>calc(s)</sub> +Q <sub>calc(d)</sub> = +2 |                   |                 |                     |                                       |                 |           |

$$(*)\Delta\Delta\text{SCF} = k^0Q^0 - kQ + Q_{\text{calc(s)}}R_{1(s)}^a + Q_{\text{calc(d)}}R_{1(d)}^a$$

$$\Delta\Delta\text{SCF}(\text{Cu}^{2+} - \text{Cu}) = 30.514 = k_{\text{Cu}}^0 \times 2 + R_{1(s)}^a + R_{1(d)}^a, \text{ then } k_{\text{Cu}}^0 = 13.4 \text{ eV and } r_{\text{Cu}^0} = 1.07 \text{ \AA}.$$

$$\Delta\Delta\text{SCF}(\text{Cu}^+ - \text{Cu}) = 9.751 = k_{\text{Cu}}^0 \times 2 - k_{\text{Cu}^+} + R_{1(s)}^a, \text{ then } k_{\text{Cu}^+} = 18.3 \text{ eV and } r_{\text{Cu}^+} = 0.787 \text{ \AA}.$$

$$\Delta\Delta\text{SCF}(\text{Cu}^{2+} - \text{Cu}^+) = 20.763 = k_{\text{Cu}^+} + R_{1(d)}^a, \text{ then } k_{\text{Cu}^+} = 18.4 \text{ eV and } r_{\text{Cu}^+} = 0.784 \text{ \AA}.$$

Considering the information contained in  $\Delta\alpha'/2$ , according to Eq.(14), we can now estimate the two parts of the relaxation energies R<sup>a</sup> and R<sup>ea</sup> separately since R<sup>a</sup> = - Q<sub>calc</sub>•R<sub>1</sub><sup>a</sup> gives the atomic part and the difference to  $\Delta\alpha'/2$  (i.e. R<sup>ea</sup> =  $\Delta\alpha'/2 + Q_{\text{calc}}\cdot R_{1}^a$ ) the extra-atomic one.

Fig.8a shows the two parts in comparison for the Zn compounds as an example. With growing cationic charge the total relaxation decreases and so does the atomic and - to a lesser extent - the extra-atomic part of it. This is to be expected since the tendency to retain electrons in an atomic interaction depends on the electronegativity relation, and a growing  $\Delta EN$  is correlated with the charge. Furthermore, we see that the relation between the two contributions changes continuously with growing charge. The halides differ very little from the chalcogenides, and there is a linear relation between both relaxation terms and the charge.

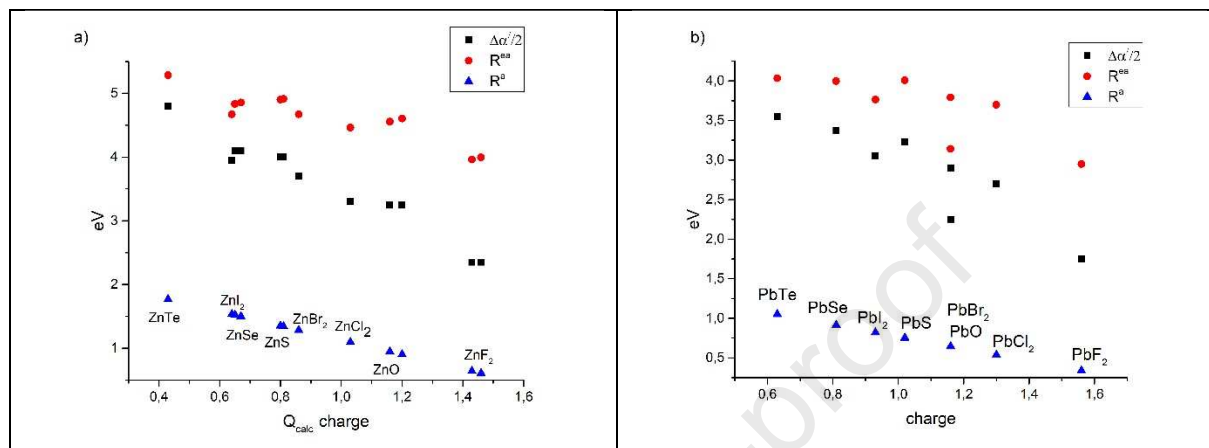


**Fig.8** A comparison between atomic and extra-atomic relaxation energies with measured differences of Auger parameters with respect to the free atom for a) Zn compounds and b) Pb compounds.

This is to be compared with the relaxation in Pb compounds where we may expect differences. Fig.8b gives the corresponding plot. The general aspect of the relaxation for Pb compounds is quite the same as for the Zn compounds, except that the span of values for the total relaxation and for  $R^{ea}$  is distinctly smaller (compare scales). The difference between halides and chalcogenides is now a little larger. However, there is one clear distinction. PbO and PbBr<sub>2</sub> have about the same cationic charge, but for the oxide the total relaxation energy and its extra-atomic part are both distinctly smaller, whereas the atomic relaxation energy fits smoothly into the general trend in these compounds. We notice again the special effect of the lone pair which strongly biases the “interaction” with neighbouring ligands.

The corresponding plots for a set of Cu compounds are given in Fig.9 where we have highlighted the two formal oxidation states.

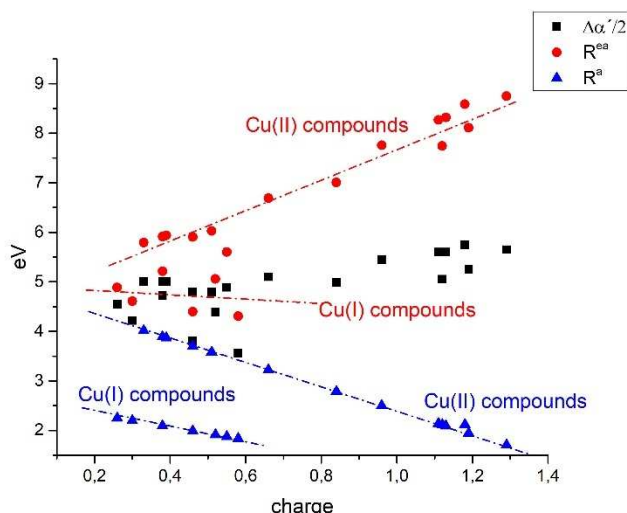


Fig.9 A comparison of atomic and extra-atomic relaxation energies with measured differences of Auger parameters for Cu compounds

These plots differ considerably from the other ones. Here we focus on the difference between the oxidation states. The total relaxation (black squares) changes very little with increasing charge (see the energy scale). Values for  $R^a$  are assembled together on the lines in the lower part of the diagram where we see a great difference between Cu(I) and Cu(II) compounds.  $R^{ea}$  values for the chalcogenides and the halides of Cu(I) (red balls) are assembled slightly below and above the line describing their trend respectively. The picture is completely different for the Cu(II) compounds. The total relaxation - and especially the extra-atomic part of it - increases with cationic charge. The 3d open shell configuration clearly changes the  $R^a/R^{ea}$  relation in these compounds.

When looking at the general trend of the relaxation energies for the Zn and Pb compounds we observe that their contribution decreases with  $Q_{calc}$ . The total electronic system seems to “stiffen” with increasing charge. The same is true for the atomic relaxation part of both Cu(I) and Cu(II) compounds. However, the extra-atomic relaxation  $R^{ea}$  is hardly affected by the charge for the Cu(I) compounds - we see an almost horizontal line describing their trend with the chalcogenides slightly above and the halides slightly below it - whereas this extra-atomic contribution increases considerably which growing charge in the case of the Cu(II) compounds. *As expected, the open shell systems are definitely more prone to external influences.*

A simple model that correlates the Auger parameter shift with the ground state Bader valence charge has been developed and applied by us to Cu(I) and Cu(II) compounds and to Ba(II), Pb(II) and Zn(II) compounds [25]. The model is able to estimate in a good approximation the slope of the  $\Delta\alpha'$  vs.  $Q_{calc}$  linear relationship for the closed shell Cu(I), Ba(II), Pb(II) and Zn(II) ions. The Auger parameter shift for the open shell Cu(II) compounds is instead independent of  $Q_{calc}$  and close to the  $(\alpha'_{Cu(s)} - \alpha'_{Cu(g)})$  value.

## 5.4 Work functions

Many years ago, Shirley [see 6 and 9b, p.140] stated: “The deduction of atomic charge in solids from core-level shifts is very elusive. The shifts are small, there is no suitable reference

level, and relaxation effects may be important. A much more promising approach lies in the analysis of the most tightly bound valence orbitals in simple solids. For binary solids such as the III-V and II-VI compounds the second and the third valence peaks are separated by an “antisymmetric gap” that is closely related to the ionicity (Pollak et al. Phys. Rev. Letters 1972, vol. 29, p. 1103”).

It is evident that our approach, i.e. the use of Eqs. (1d, 6 and 14) in a sort of retro-calculation (see Conclusion), may represent an advancement in the direction of the deduction of the atomic charge in solids from core-level shifts. A crucial point, however, is the knowledge of the term describing the work function.

With good electrical contact of the sample to the spectrometer charging effects play no role in the case of metals. Photoelectrons must nevertheless have certain energies to pass the surface of the sample into vacuum. The term “work functions” describing such energies is nowadays used not only for metals but for all kinds of samples. The physical mechanisms for this retarding effect on outgoing electrons are complex and may be classified into bulk and surface contributions, the former having to do with the energetics of the total electronic system and the latter with the special surface features of the diverse crystallites which make up the sample. Structural relaxations and reconstructions in part of the atomic arrangements will induce local dipoles which will interact with the outgoing photoelectrons, and this will even lead to varying work functions for different faces of single crystals.

The work functions of insulating or semiconducting solids are generally not known. In principle there are ways to access work functions experimentally by varying an electric field between sample and detector entrance so as to slow down or stop the movement of the emitted electrons in a controlled manner. Furthermore, the low energy cut-off of kinetic energies of the outgoing electrons in comparison with the energy  $h\nu$  of the impinging radiation will give an estimate for  $\Phi$  (for metallic samples!). Meanwhile many work functions for metals have been tabulated,  $\Phi$  values are even given for different crystallographic surface layers of single crystals. However, such investigations are generally tedious, and therefore experimental work functions are not available for many compounds. It was therefore necessary to find ways to predict them using other known experimental parameters.

Theories how to define bulk work functions have been known since quite a long time [26-30]. The basic concept of such approaches is the assumption that the retarding effect on photoelectrons may be compared with the tendency to attract electrons in a bonding interaction between atoms, i.e. the electronegativities of the elements sum up to a specific bulk effect in the solid when we assume that there is a sort of electronegativity equalization between all the atomic components, and that - according to Density Functional Theory - the electronegativity may be seen as the negative of the chemical potential of the electrons [31].

Chen et al. [27] reported an empirical and remarkable relationship between the metal work function and the absolute electronegativity of Mulliken of a free metal atom in the gaseous state,  $\Phi_M \approx \chi_M$ . The absolute electronegativity is calculated as the average of the ground state first ionization energy and the electron affinity energy ( $\chi = (I_1 + A)/2$ ). The same authors describe an empirical relationship useful to estimate the work function of insulating and semiconducting solids as first reported by Nethercot [28]: the Fermi energy of binary compounds, MX, can be taken as the geometric mean of the electronegativities of the two components,  $E_F^{\text{th}} = \chi_M \chi_X^{1/2}$ . It is important to notice that  $E_F^{\text{th}}$  is then determined solely by the electronegativities of the constituent elements and is hence not structure or coordination sensitive, and that is - in our opinion - a weak point in this approach.

The same relationship was also used by Poole et al. [29] to estimate the work function of  $\text{MX}_2$  compounds employing atomic electronegativities from the scales proposed by Pauling and by Sanderson. We may recall that the electronegativity scales proposed by Mulliken and Sanderson, as well as scales proposed by other authors, are to a good approximation linearly related to the scale of Pauling [31]. For our purposes we use the relation proposed by Chen et al. to estimate the work function of all the solids studied with our model.

The relation to the experimental measurements described above may be explained by the photoelectric threshold energy defined by  $E_t^{\text{th}} = E_F^{\text{th}} + \frac{1}{2} E_g$  and representing the electrons ejected from the maximum of the valence band.  $E_g$  is the experimental band gap energy to be measured by other spectroscopic methods. In the case of a metal A the band gap  $E_g = 0$ , so

$$E_t^{\text{th}} = E_F^{\text{th}} = \chi_A = \Phi.$$

Since experimental work functions of metals were first to be known their relationship to electronegativities was first noticed, and this led to the theories described here. Fig.10 presents the relations of the described terms for different materials in a schematic plot. It is common use to locate the Fermi level in semiconductors in the band gap at a position where there is a 50% probability to find an electron in a specific energy state.

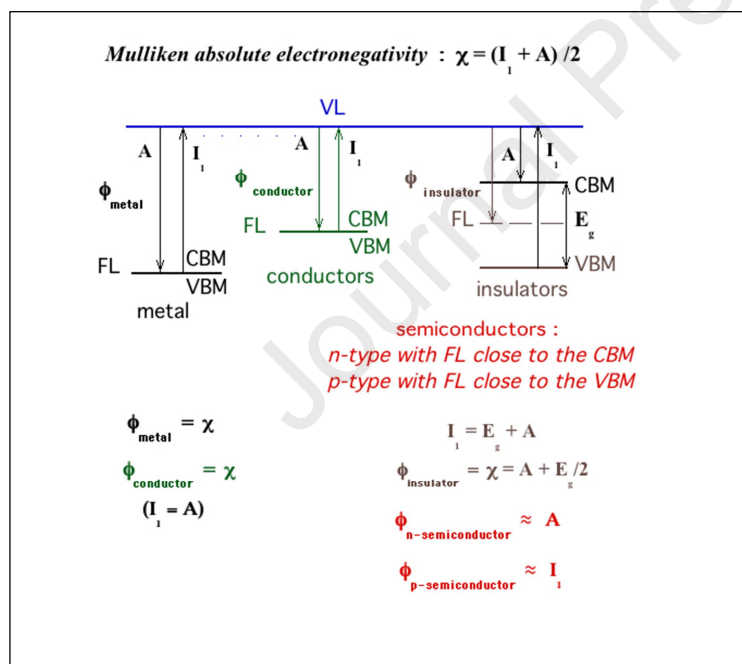


**Fig.10** Scheme representing the position of the vacuum level and the Fermi level on an energy scale. (Note that  $E_F^{\text{th}} = \Phi$  for the metal and for conductors and that for insulators and semiconductors  $E_t^{\text{th}} = I_1 = \Phi + \frac{1}{2} E_g$ , i.e.  $\Phi = I_1 - \frac{1}{2} E_g = A + \frac{1}{2} E_g$ )

We now try to use this approach to estimate the missing element  $\Phi$  in our theory. In Appendix C (Supplement) we report the Mulliken electronegativities of the component elements and their geometric mean of the components of each studied solid. It is assumed that according to the principle of electronegativity equalization the work function of the  $\text{MX}_n$  solid is given by  $\Phi_{\text{MX}_n} \approx (\chi_M \chi_X^n)^{1/(n+1)}$ . These values may be then used as a crude estimate in the calculations according to Eq.(1a). However, as described in the following paragraph, we propose to apply them in a slightly different context.

## 6 Conclusion

Many spectroscopic experiments such as NMR or Mössbauer spectroscopy deal with so-called chemical shifts where typical atomic states and the energy differences between them are influenced by the interactions with surrounding atoms, and their interpretation is based on sound theories since long times. In photoelectron spectroscopy, too, the binding energies  $E_b$  of electrons originating from different energy states can vary considerably for the same atomic species depending on their embedment in different matrices. At a first glance such chemical shifts seem to follow known trends such as electronegativity differences or polarizabilities of neighbouring atoms. However, the correlations are not all univariate, and plots of binding energies or Auger electron energies versus such parameters very often present an unintelligible scatter as demonstrated in the discussion of the Wagner plots above.

Since the pioneering work of Kai Siegbahn there have been several approaches to found a theoretical basis of understanding [see Ref.1 and references therein] of such chemical shifts. By a generalization of previous approaches [2a, 6] one of us has presented a simple theoretical model some time ago [3-5] combining several parameters which can influence the energy of the outgoing electrons in a unifying equation such as the one presented in the introductory paragraphs of this paper where so-called initial state effects and final state effects are combined and the free atom data are taken as a natural reference for the core electron binding energy shift (Eq.(1b)):

$$E_b(c_i)^{FL}(\text{atom/solid}) = E_b(c_i)^{VL}(\text{free atom}) + Q^0(k^0 - k) + kQ_{\text{calc}} + V_M - \Phi_{\text{solid}} - R(c_i),$$

and in Eq.(1c) the last term is further specified as atomic and extra-atomic relaxation energies

$$R(c_i) = -R_1^a \cdot Q_{\text{calc}} + R^{\text{ea}}(\text{extra-atomic}).$$

In the work presented here we try to “feed” the diverse terms of such equations with the results of theoretical DFT calculations in order to test the validity of this theoretical approach. To do so we have chosen a series of compounds of Ba, Zn, Pb and Cu which represent different types of electronic states on the one hand and which mostly crystallize in simple structures with few crystallographic sites on the other hand. By calculating Bader charges, atomic volumes and site potentials (and therefore the local Madelung energy term) for chalcogenides and halides of these elements we have produced a data basis to rationalize the spread of measured binding energies and Auger energies in comparison with the results of this theory.

It has thereby become possible to quantify different factors separately which bias the kinetic energies of the outgoing electrons termed initial state (ISE) and final state effects (FSE) (see Fig.1). Special attention was thereby directed to the interplay of electron numbers and electron densities in the valence shell with the leaving electrons described by such terms as  $kQ$  (atom/solid) or  $k^0Q^0$  (free atom) with the ground state valence charge given by  $Q_{\text{calc}} = Q^0 - Q$ . As a second key aspect we have investigated the influence of site potentials as derived by Madelung-type calculations on the basis of the Bader charges, and finally we use the information contained in the shift of the Auger parameter to estimate the atomic and extra-atomic relaxation energies (see Eq.(11)). The change of the binding energies of the single atoms in the gaseous state to those in the diverse compounds can thereby be attributed to several distinct influences. Two of these parameters ( $kQ$  and  $V_M$ ) vary strongly with the charge of the atom, which clearly has the strongest effect on the chemical shift in XPS and AES (see Appendix D and Fig.11 in the Supplement).

## A proof of principle

In the following we present a sort of “crucial test” for the validity of our fundamental equation. Fig.12 may give a pictorial presentation of the effect of the different “correction terms” in our unifying equation by reversing the “movement” insinuated in Fig.1 from  $E_{b(g)}^{V\text{Lexp}}$  to  $E_{b(s)}^{FL\text{exp}}$  in solving this equation the other way round for the Zn compounds as an example, i.e. “moving back” the energy values measured for the solids in the direction of the gaseous state. The arrows from the ticks of the measured energies ( $E_b(\text{exp})$ , black squares) to the ones “corrected” by ISE and FSE ( $E_b(g)(\text{calc})$ , red circles) are all correctly directed towards the  $E_b(g)$  value at about 1029 eV. A last step would add the contribution of the work functions to give values which should be close to the binding energy for Zn in the gaseous state.

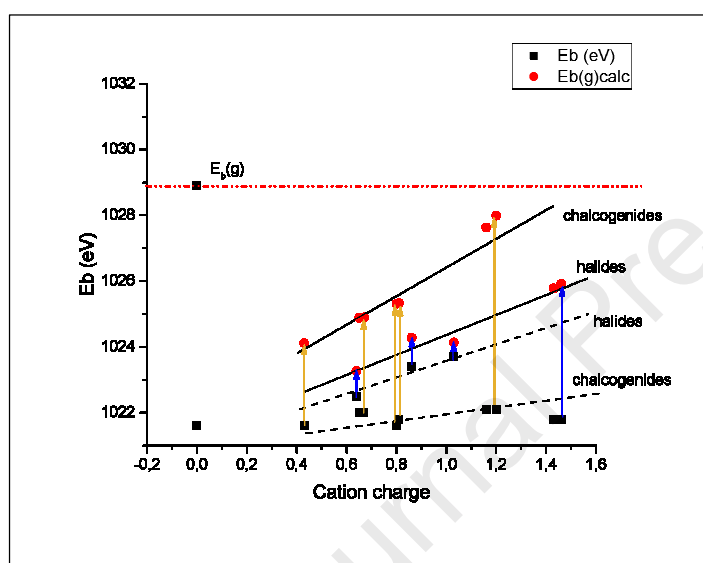


**Fig.12** The shift of real measured binding energies (black squares) towards the binding energy value of the free Zn atom  $E_b(g)$  by application of the corrections terms of Eq.(1c) (red circles) (see text).

It is interesting to note that the two series of compounds respond differently to the application of the diverse terms of our equation. For the chalcogenides the terms  $kQ_{\text{calc}}$  and  $V_M$  in Eq.(1c), related to the charge, volume and site potential, all move the measured binding energies closer to that of the free atom than in the case of the halides (excepting  $\text{ZnF}_2$ ). On the average the potentials are higher for the halides. However, the geometric factors are lower, so the advantage of higher potentials is evidently counteracted - at least in part - by the topology of the structures. The gap between the “calculated fictitious”  $E_b(g)$  value and the measured one closes for both series of compounds when moving to higher charges of the Zn cation (equivalent to higher  $\Delta\text{EN}$ ), and the two series behave differently with regard to the size of the missing gap and the gradient of the lines. This behaviour may be explained by looking at the Figs.5 and 7c in our paper.

We find the Zn halides in the  $\Delta > 0$  field and the chalcogenides in the  $\Delta < 0$  region. We have stated that the two terms  $kQ_{\text{calc}}$  and  $V_M$  counteract and partly balance each other. For the Zn halides the  $1/r$  term wins, so the effect of  $V_M$ , i.e. the effect of the local potential at the cation site, is weakened. The overall correction is reduced and less dependent on the potential term.

This leads to the line for the halides being below the other one in our Fig.12 and less steep in the diagram.

When finally adding the contribution of the work functions as defined in the foregoing paragraph we do approach the  $E_{b(g)}^{(VLexp)}$  value. Furthermore, the difference between the two lines joining either the chalcogenides or the halides (not plotted here) has almost disappeared. However, in many cases we overshoot the experimental value for the binding energy of the single atom more and more with increasing cationic charge, and this is to be expected since these work functions increase, whereas the remaining gap mentioned before decreases with charge. So, this merits a closer look at the way we introduce the WFs calculated from the Mulliken electronegativities.

As said above it is common use to formally locate the Fermi level in semiconductors in the band gap at a position where there is a 50% probability to find an electron in a given energy state, The definition of the threshold value by Chen and Nethercot as  $E_t^{th} = E_F^{th} + \frac{1}{2} E_g$  fixes the Fermi level halfway between the valence band maximum (VBM) and the conduction band minimum (CBM), and therefore its position is marked in the middle of the band gap in Fig.10. However, as indicated in this plot, its position depends on the type of material and it may vary in the gap between the VBM and the CBM depending on the semiconductor type. For p-type compounds the “distance” to the vacuum level will be larger by up to  $\frac{1}{2} E_g$  and for n-type ones it will be even smaller by up to  $\frac{1}{2} E_g$  than from the level halfway in between. We therefore propose to use the “Mulliken” values for work functions in a different way. The following Fig.13 gives a selection of Cu compounds - as an example - where we compare known values for  $E_{b(g)}^{VL}$  with those calculated first by our retro-calculation including the “Mulliken  $\Phi$ ” and then also by using such a kind of “adapted” work function depending on the type of semiconductor.

The black squares give the experimentally measured binding energies and the red circles give a fictitious  $E_{b(g)}^{VL}$  value resulting from a retro-calculation including the Mulliken work function. The arrows show the shift to “corrected”  $E_{b(g)}^{VL}$  values (blue triangles) when assuming the compounds to be n-type (as for the Zn and Pb compounds) or p-type semiconductors (as for the Cu(I) compounds). (Results of such calculations for all the compounds under study in this paper are given in the table and in additional graphs in Appendix E in the Supplement.)

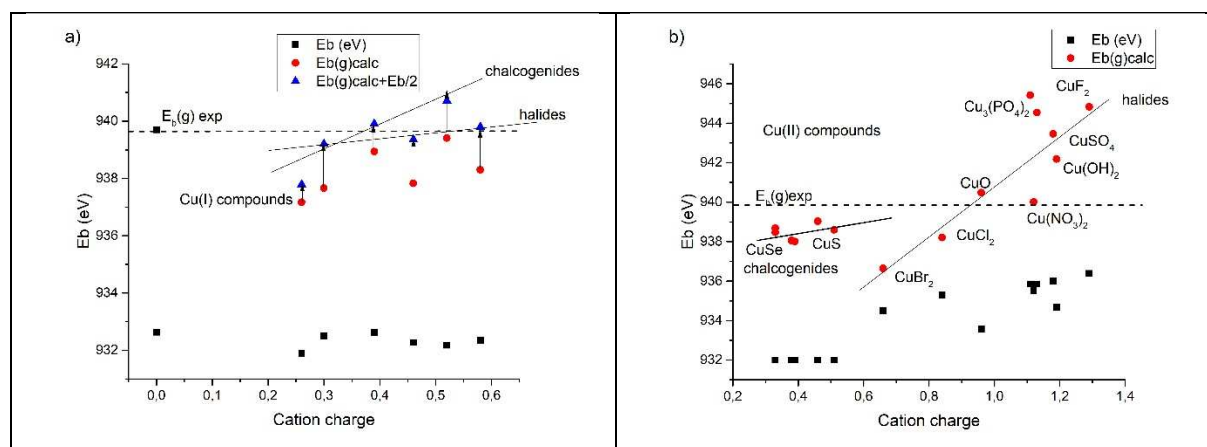


**Fig.13** A comparison of experimental binding energies for gaseous single atoms  $E_{b(g)}^{VL}$  and the respective values resulting from a retro-calculation for a) Cu(I) (blue triangles) and b)



Cu(II) compounds. (See text!) The “correction arrows” are shown when band gap values were known. These results are also presented in a tabular form in the Appendix E (Supplement).

For the Cu(I), Zn and Pb compounds our corrected values now line up quite satisfactorily with the experimental value as shown in Fig.13 a (and c and d in Appendix E in the Supplement) respectively. For Zn and Pb the fit is best for the correction by  $-\frac{1}{2} E_g$ , i.e. assuming an n-type material. For the Cu(I) compounds we must add  $\frac{1}{2} E_g$ . We could therefore venture to say that such a detailed analysis of the XPS spectra including an experimental work function would probably allow a prediction of the type of semiconductor.

This is not true for the series of Cu(II) compounds. The corresponding graph in Fig.13 b does not include values resulting from an additional correction by the position of  $E_F$  in the band gap. The chalcogenides CuS and CuSe surprisingly fit better than the other compounds even without any further correction. In fact, the magnetic measurements and the Cu2p XPS spectra show that in these compounds Cu is virtually in the oxidation state +1, and a close inspection of the structure shows up some very short S-S distances also indicating a partial oxidation of the anion lattice.

The deviation of the other compounds amounts up to  $\pm 4$  eV, which is more than the possible band gap correction applied in the other cases. Looking at the structures we find highly anisotropic surroundings for the  $\text{Cu}^{2+}$  cation mostly in the form of a square planar arrangement or in tetragonally distorted octahedra.

It may be assumed that such results for the retro-calculations are due to the open shell configuration of these Cu(II) cations. There is one term in our fundamental equation which is prone to effects of a non-radial electron distribution. We have introduced the terms  $k^0Q^0$  and  $kQ$  as factors describing the shielding of the charge of the nucleus by valence electrons, and we have pointed out above that the  $ns^2$  configuration in some Pb(II) compounds (especially in PbO) leads to unusual experimental binding energies when there is a pronounced lone pair eccentricity. A similar effect may influence the open shell systems where the total electron configuration is not radial-symmetric. We therefore propose to consider such effects by a formal reduction of shielding power in a modified term  $k(Q-\epsilon)$  for such cases. In a retro-calculation the position of the “band gap corrected value” will then move up less in our graphs in Fig.13. It would be ever so interesting to derive the term  $\epsilon$  from a close comparison with experimental data, however, it does not make sense to start this study as long as we are forced to rely on such crude data resulting from the estimation of work functions from Mulliken electronegativities. To really evaluate our approach we need binding energies from XPS and AES experiments and experimental work functions derived from measurements on the same instrument. We would like to encourage experimentalists to produce this important information and we hope to find such data in the near future.

To finish our “Conclusion” we may point out that our fundamental equation has successfully been used also in other contexts. In previous work [25] we reported  $\Delta\alpha'$  vs.  $Q_{\text{calc}}$  plots for the same Cu(I), Zn(II), Ba(II) and Pb(II) samples (as reported above such a plot for Cu(II) compounds is to a good approximation a line parallel to the x-axis). Our simple model presented in Ref. 25 links the Auger parameter shift with the local ground valence charge obtained by DFT calculations and the Bader charge analysis code. This is an important achievement because - as said above - the Auger parameter may be easily measured even on samples prone to charging phenomena (insulators and semiconductors). It is also independent of the reference level employed to measure the electron kinetic energies of core and Auger electrons (the Fermi or the vacuum level). The local valence charge, on the other hand,

represents a valuable piece of chemical knowledge, and its determination has been an objective of X-ray photoelectron spectroscopy (ESCA) since the early days of its discovery [Ref.1 and references therein].

All in all, we see that there is a delicate balance of different terms adding up in a calculation of binding energies whose results cannot be foreseen. Their contribution and balance are responsible for the - sometimes unintelligible - scatter of data in Wagner plots, and their substantiation - as presented in this paper - could help to rationalize the results. It may be surprising that the topology of the individual structures plays such a large role in the balance of the different terms of our equation. In the paragraph devoted to such topics (5.2) we have demonstrated how the local effect of electron density at an atom on the one hand and a potential built up from a collective arrangement of charge points in a certain topology on the other hand interact to a combined initial state effect. We have demonstrated that this topological effect can also be described more clearly by contrasting it in the form of so-called geometric factors with the respective electron density given as reciprocal sizes of the electron clouds.

We may summarize that the results of DFT calculations help to demonstrate the bearing of our unifying equation which describes the influences of several factors on binding energies and kinetic energies of Auger electrons. This kind of scientific cross-breeding opens up new possibilities to rationalize the spread of XPS and AES data of the same element in different compounds.

## References

- [1] a) W.F. Egelhoff Jr., Core-level binding-energy shifts at surfaces and in solids, *Surf. Sci. Rep.* 6 (1987) 253-415. b) S. Hüfner, *Photoelectron Spectroscopy, Principles and Applications*, Third Edition, Springer 2003
- [2] a) J.Q. Broughton, P.S. Bagus,  $\Delta$ SCF calculations of free atom-ion shift, *J. Electron Spectr. Related Phenom.* 20 (1980) 127-148. b) P. S. Bagus, E. S. Ilton, C. J. Nelin, The interpretation of XPS spectra: Insights into materials properties, *Surf. Sci. Rep.* 68 (2013) 273-304.
- [3] G. Moretti, Auger parameter and Wagner plot in the characterization of chemical states by X-ray photoelectron spectroscopy: a review, *J. Electron Spectr. Related Phenom.* 95 (1998) 95-144.
- [4] G. Moretti, The Wagner plot and the Auger parameter as tools to separate initial- and final-state contributions in X-ray photoelectron spectroscopy, *Surface Science* 618 (2013) 3-11.
- [5] G. Moretti, A. Palma, E. Paparazzo, M. Satta, Auger parameter and Wagner plot studies of small copper clusters, *Surface Science* 646 (2016) 298-305.
- [6] C.S. Fadley, S. B. M. Hagstrom, M. P. Klein, D. A. Shirley, Chemical effects on core-electron binding energy in iodine and europium. *J. Chem. Phys.* 48 (1968) 3779-3794.
- [7] a) C.D. Wagner, *Faraday Discuss. Chem. Soc.*, Chemical shifts of Auger lines, and the Auger parameter, 60 (1975) 291-300; b) C.D. Wagner, A. Joshi, The Auger parameter, its utility and advantages: a review, *J. Electron Spectr. Related Phenom.* 47 (1988) 283-313.

- [8] J. E. Castle, D. Epler, Chemical shifts in photoexcited Auger spectra. Proc. R. Soc. Lond. A 339 (1974) 49-72.
- [9] a) D.A. Shirley, Relaxation effects on Auger energies. Chem. Phys. Lett. 17 (1972) 312-315; b) D.A. Shirley, ESCA. Results versus other physical and chemical data, J. Electron Spectr. Related Phenom. 5 (1974) 135-148.
- [10] G. Hohlneicher, H. Pulm, H.-J. Freund. On the separation of initial and final state effects in photoelectron spectroscopy using an extension of the Auger-parameter concept. J. Electron Spectr. Related Phenom. 37 (1985) 209-224.
- [11] NIST X-ray Photoelectron Spectroscopy Database, Version 4.1 (National Institute of Standards and Technology, Gaithersburg, 2012); <http://srdata.nist.gov/xps/>. (Accessed 21 October 2019).
- [12] a) G. Moretti, F. Filippone, M. Satta, Use of Auger parameter and Wagner plot in the characterization of Cu-ZSM-5 catalysts, Surface Int. Anal. 31 (2001) 249-254; b) G. Moretti, The Auger parameter, in Surface Analysis by Auger and X-ray Photoelectron Spectroscopy, Chapter 18, Ed. by D. Briggs, J.T. Grant, 2003, IM Publications, pp.501-530; c) M. Satta, S. Morpurgo, G. Moretti, Long range and surface effects on the Auger parameter: electrostatic self consistent polarization energy model, Surface Int. Anal. 40 (2008) 692-694; d) M. Satta, G. Moretti, Auger parameter and Wagner plots, J. Electron Spectr. Related Phenom. 178-179 (2010) 123-127.
- [13] a) I.A. Abrikov, W. Olovsson, B. Johansson, Valence-band hybridization and core level shifts in random Ag-Pd alloys, Phys. Rev. Lett. 87 (2001) 176403(1-4); b) W. Olovsson, I.A. Abrikov, B. Johansson, A. Newton, R.J. Cole, P. Weightman, Auger energy shifts in fcc AgPd random alloys from complete screening picture and experiment, Phys. Rev. Lett. 92 (2004) 226406(1-4); c) W. Olovsson, T. Marten, E. Holmström, B. Johansson, I.A. Abrikov, First principle calculations of core-level binding energy and Auger kinetic energy shifts in metallic solids, J. Electron Spectr. Related Phenom. 178-179 (2010) 88-99.
- [14] J.Q. Broughton, P.S. Bagus, A study of Madelung potential effects in the ESCA spectra of the metal oxides, J. Electron Spectr. Related Phenom. 20 (1980) 261-280 and (Errata) 21 (1980) 283-284.
- [15] H. Wadati, A. Maniwa, A. Chikamatsu, H. Kumigashira, M. Oshima, T. Mizokawa, A. Fujimori, and G. A. Sawatzky, Madelung potentials and covalency effect in strained  $\text{La}_{1-x}\text{Sr}_x\text{MnO}_3$  thin films studied by core-level photoemission spectroscopy, Physical Review B (2019) 80, 125107-125111.
- [16] G. Kresse and J. Furthmüller, Efficient iterative schemes for ab initio total-energy calculations using a plane-wave basis set, Phys. Rev. B 54 (1996) 11169-11186.
- [17] G. Kresse, J. Furthmüller, Efficiency of ab initio calculations for metals and semiconductors using a plane wave basis set, Comput. Mater. Sci. 6 (1996) 15-50.
- [18] P. E. Blöchl, Projector augmented-wave method, Phys. Rev. B 50 (1994) 17953-17979.
- [19] J. P. Perdew, K. Burke, M. Ernzerhof, Generalized gradient approximation made simple, Phys. Rev. Lett. 77 (1996) 3865-3868.

- [20] P. E. Blöchl, O. Jepsen, O. K. Andersen, Improved tetrahedron method for Brillouin-zone integrations, *Phys. Rev. B* 49 (1994) 16223–16233.
- [21] R. F. W. Bader, *Atoms in Molecules: A Quantum Theory*, Oxford University Press, New York, 1990.
- [22] G. Henkelman, A. Arnaldsson, and H. Jónsson, A fast and robust algorithm for Bader decomposition of charge density, *Comput. Mater. Sci.* 36 (2006) 254-360.
- [23] T. Beyer, H. P. Beck, Lattice Potentials as an Instrument in Crystal Chemistry, Part I, Theory and Calculation, *Z. Krist.* 212 (1997) 559-564.
- [24] Shannon, R. D., Revised Effective Ionic Radii and Systematic Studies of Interatomic Distances in Halides and Chalcogenides". *Acta Crystallogr. A* 32 (1976) 751–767.
- [25] G. Moretti, H. P. Beck, Relationship between the Auger parameter and the ground state valence charge of the core ionized atom: The case of Cu(I) and Cu(II) compounds. *Surf. Interface Anal.* 51 (2019) 1359-1370. 2019.
- [26] H. B. Michaelson, The work function of the elements and its periodicity, *J. Appl. Phys.*, 48 (1977) 4729-4733.
- [27] E.C.M. Chen, W.E. Wentworth, J.A. Ayala, The relationship between the Mulliken electronegativities of the elements and the work functions of metals and non-metals, *J. Chem. Phys.* 67 (1977) 2642-2647.
- [28] A.H. Nethercot, Jr, Prediction of Fermi energies and photoelectric thresholds based on electronegativities Concepts, *Phys. Rev. Lett.* 33 (1974) 1088-1091.
- [29] R.T. Poole, D.R. Williams, J.D. Riley, J.G. Jenkin, J. Liesegang, R.C.G. Leckey, Electronegativity as a unifying concept in the determination of Fermi energies and photoelectric thresholds, *Chem. Phys. Lett.*, 36 (1975) 401-403.
- [30] R. G. Parr, W. Yang, *Density-Functional Theory of atoms and molecules*, Oxford University Press, New York, 1989.
- [31] J. Mullay, Estimation of atomic and group electronegativities, in *Electronegativity*, Editors: K.D. Sen and C. K. Jørgensen, *Structure and Bonding* 66 (1987)1-25, Springer-Verlag Berlin Heidelberg, Germany.
- [32] W. H. Strehlow, E. L. Cook, Compilation of energy band gaps in elemental and binary compounds, *J. Phys. Chem. Ref. Data*, 2(1973) 163-199

## Supplement

### Appendix A: On the derivation of the terms $k^0Q^0$ and $kQ$ in the Eqs. (1a and 1b) and the previous approach by Broughton and Bagus.

This appendix is aimed to illustrate in more detail some terms of Eq.(1a and 1b) taking the influence of the electron cloud into account of both the free atom and the atom in a solid respectively on the leaving photoelectron, and it also considers the site potential induced by the charge distribution of the surrounding atoms in the solid – all being aspects of the initial state effects. The terms  $k^0Q^0$  and  $kQ$  result from a simplistic model of the shell-like charge distribution in the electron cloud of an atom assuming them in conducting spheres with radius  $r_1, r_2, r_3, \dots$ , up to the “valence” sphere with radius  $r_0$ . Each sphere has a negative charge according to the respective number of electrons in it up to the “valence” sphere with charge  $-Q^0e$ . According to the Gauss’ theorem, the potential within an individual sphere (say: number 3) is

$$V_3 (\text{free atom}) = (1/4\pi\epsilon_0)[(+ Q_n - Q_1 - Q_2 - Q_3) e/r_3 - Q_4e/r_4 - \dots - Q^0 e/r_0]$$

and the “binding energy” for the electron in the sphere number 3 will therefore be

$$E_b (3, \text{free atom}) = eV_3(\text{free atom}).$$

Charge ( $e$ ) and radius ( $r$ ) may be combined in the form of  $k_i$  values ( $i = 3, 4, \dots, 0$ ) and written as

$$k_i (\text{joule}) = (e^2/4\pi\epsilon_0)/r_i \text{ and } k_i (\text{eV}) = 14.4 (\text{eV}\text{\AA})/r_i (\text{\AA}).$$

Applying the same approach to a positive ion ( $Q < Q^0$ ) the potential at the sphere number 3 will be

$$V_3 (\text{free ion}) = (1/4\pi\epsilon_0) [(+ Q_n - Q_1 - Q_2 - Q_3) e/r_3 - Q_4 e/r_4 - \dots - Q e/r]$$

where the number of terms is the same as before, but the radius of the outermost shell is now different ( $r < r_0$ ). The shift of the binding energy (ion vs. atom) of an electron emitted from shell number 3 will therefore be

$$E_b(3, \text{free ion}) - E_b(3, \text{free atom}) = eV_3 (\text{free ion}) - eV_3(\text{free atom}) = -kQ + k^0Q^0,$$

and this is included in Eq.(1a) to allow for the shielding effect of the different number of electrons in both cases.

The Eqs. (1a and 1b) are a generalization of previous equations suggested by Broughton and Bagus [2a]. These authors describe the core-level ionization potential IP of an atom A as follows:

$$\begin{aligned} IP_A &= -\epsilon_{nlA} - (E_{cA} + kq_A + E_{\text{flow}A}) \\ \epsilon_{nlA} &= \epsilon_{nlA}(\text{gas}) + bq_A + E_{MA} \end{aligned}$$

According to them  $IP_A$ , may be calculated considering the following contributions :

- $\epsilon_{nl}$  is the eigenvalue of the core level  $nl$  (obtained from a Hartree-Fock calculation on the molecule or bulk material);
- $E_{cA}$  is the local contraction energy on the neutral atom A;
- $E_{\text{flow}A}$  is the extra-atomic relaxation (or polarization) energy;

-  $kq_A$  is a correction term for the amount of charge in the valence levels of atom A,  $k$  being assumed constant and  $q$  being the charge on the atom;

The last three terms on the right-hand side of Eq.(1d) are collectively termed “relaxation energy”, and of these terms,  $E_c$  is approximated by the local or gas-phase atomic relaxation energy. The eigenvalue, Eq.(1e), mirrors initial-state effects such as the charge on the ionized atom and Madelung potentials, while the IP includes both initial-state and final-state (i.e. polarization) effects:

-  $\epsilon_{nlA}(\text{gas})$  is the gas-phase, neutral-atom eigenvalue;

-  $E_{MA}$  is the potential on atom A due to its environment (often approximated in bulk systems by the Madelung potential);

-  $bq_A$  is a correction term for the charge  $q$  on the atom ( $b$  being assumed constant).

### Appendix B: Application of Eq.(1d) to several cases that may be of interest.

Eq.(1d) is related to the atom in a solid sample (that may be in general metallic, semiconducting and insulating):

$$E_b(c_i)^{FL}(\text{atom/solid}) = E_b(c_i)^{VL}(\text{free atom}) + Q^0(k^0 - k) + kQ_{\text{calc}} + V_M - \Phi_{\text{solid}} + R_1^a \cdot Q_{\text{calc}} - R^{ea}(\text{extra-atomic})$$

As for the atom in the metal solid ( $Q = Q^0$  and  $R_1^a \cdot Q_{\text{calc}} = 0$ ) the equation becomes

$$E_b(c_i)^{FL}(\text{atom/metal}) = E_b(c_i)^{VL}(\text{free atom}) + Q^0(k^0 - k) - \Phi_{\text{metal}} - R^{ea}(\text{extra-atomic})$$

The binding energy of the free atom referenced to the Fermi level of the spectrometer, which is in equilibrium with the Fermi level of the atom in the metal solid, may be written as

$$E_b(c_i)^{FL}(\text{free atom}) = E_b(c_i)^{VL}(\text{free atom}) - \Phi_{\text{metal}}$$

Note that in the free atom the valence charge extends well outside the core, while in a monoatomic solid it is normalized to the electrically neutral Wigner-Seitz cell. Such a compression of the valence charge into the cell corresponds to a reduction of the metal core electron binding energy (see R.E. Watson, M.L. Perlman, J.F. Herbst, Phys. Rev. B 13 (1976) 2358-2365) represented in Eq.(A1) by the term  $Q^0(k^0 - k)$ , with  $k > k^0$  because the atomic radius of the atom in the solid metal is less than the atomic radius of the free atom ( $r < r^0$ ).

The binding energy for a free ion, considering all the  $Q^0$  valence electrons removed, becomes

$$E_b(c_i)^{VL}(\text{free ion}) = E_b(c_i)^{VL}(\text{free atom}) + k^0 Q^0 - R(c_i)$$

$$\text{where } R(c_i) = -R_1^a \cdot Q^0$$

The binding energy for a free ion, considering only  $(Q^0 - Q)$  valence electrons removed, becomes

$$E_b(c_i)^{VL}(\text{free ion}) = E_b(c_i)^{VL}(\text{free atom}) + k^0 Q^0 - kQ - R(c_i)$$

$$\text{where } R(c_i) = -R_1^a \cdot (Q^0 - Q) = -R_1^a \cdot Q_{\text{calc}}$$

### Appendix C: Estimation of the work function of the studied samples by the Mulliken's absolute electronegativity and the principle of the electronegativity equalization.

In the following table we report the ground state Mulliken's electronegativity of the components M, Y and X elements present in our studied samples. The geometric mean of these values, according to Refs. 27-30, can be taken as an estimate of the work function of the solid  $M_a Y_b X_n$ . This is justified within the Density-functional Theory by the principle of electronegativity equalization, meaning that by the incorporation of the free atoms into a solid the electronegativity of all the elements becomes the same and is then equal to the negative value of the chemical potential of the electrons [31]. Note the meaning of the symbols in the empirical formula: e.g. in the case of Zn compounds: Zn (M= Zn; n = 0), ZnO (X = O; n = 1), ZnF<sub>2</sub>(X = F; n = 2). (The ground state electronegativities reported by Chen et al. [28] are somewhat higher because they add half the value of the sum of the promotion energies for the ionization potential and the electron affinity attributed to a particular type of bonding, i.e. the valence state is being considered.)

| Zn, Ba and Pb compounds $MX_n$ | $\chi_M / \text{eV}$ | $\chi_X / \text{eV}$ | $\Phi_{MX_n} \approx (\chi_M \chi_X^n)^{1/(n+1)} / \text{eV}$ |
|--------------------------------|----------------------|----------------------|---|
| Zn                             | 4.452                |                      | 4.45  |
| ZnO                            |                      | 7.540                | 5.79  |
| ZnS                            |                      | 6.219                | 5.26  |
| ZnSe                           |                      | 5.887                | 5.12  |
| ZnTe                           |                      | 5.490                | 4.94  |
| ZnF <sub>2</sub>               |                      | 10.41                | 7.84  |
| ZnCl <sub>2</sub>              |                      | 8.290                | 6.74  |
| ZnBr <sub>2</sub>              |                      | 7.589                | 6.35  |
| ZnI <sub>2</sub>               |                      | 6.755                | 5.88  |
| Ba                             | 2.678                |                      | 2.68  |
| BaO                            |                      | 7.540                | 4.49  |
| BaS                            |                      | 6.219                | 4.08  |
| BaSe                           |                      | 5.887                | 3.97  |
| BaTe                           |                      | 5.490                | 3.83  |
| BaF <sub>2</sub>               |                      | 10.41                | 6.62  |
| BaCl <sub>2</sub>              |                      | 8.290                | 5.69  |
| BaBr <sub>2</sub>              |                      | 7.589                | 5.36  |
| BaI <sub>2</sub>               |                      | 6.755                | 4.96  |
| Pb                             | 3.890                |                      | 3.89  |
| PbO                            |                      | 7.540                | 5.42  |
| PbS                            |                      | 6.219                | 4.92  |
| PbSe                           |                      | 5.887                | 4.79  |
| PbTe                           |                      | 5.490                | 4.62  |
| PbF <sub>2</sub>               |                      | 10.41                | 7.50  |
| PbCl <sub>2</sub>              |                      | 8.290                | 6.44  |
| PbBr <sub>2</sub>              |                      | 7.589                | 6.07  |
| PbI <sub>2</sub>               |                      | 6.755                | 5.62  |

| Cu(I) and Cu(II) compounds $M_a Y_b X_n$        | $\chi_M / \text{eV}$ and $\chi_Y / \text{eV}$ | $\chi_X / \text{eV}$ | $\Phi_{M_a Y_b X_n} \approx (\chi_M^a \chi_Y^b \chi_X^n)^{1/(n+a+b)} / \text{eV}$ |
|---|---|----------------------|---|
| Cu  | 4.481   |                      | 4.48  |
| Cu <sub>2</sub> O                               |   | 7.540                | 5.33  |
| Cu <sub>2</sub> S                               |   | 6.219                | 5.00  |
| Cu <sub>2</sub> Se                              |   | 5.887                | 4.91  |
| Cu <sub>2</sub> Te                              |   | 5.490                | 4.79  |
| CuCl  |   | 8.290                | 6.09  |
| CuBr  |   | 7.589                | 5.83  |
| CuI   |   | 6.755                | 5.50  |
| Fe  | 4.027   |                      |   |
| CuFeS <sub>2</sub>                              |   | 6.219                | 5.14  |
| CuO   |   | 7.540                | 5.81  |
| CuS   |   | 6.219                | 5.28  |
| CuSe  |   | 5.887                | 5.14  |
| CuTe  |   | 5.490                | 4.96  |
| CuF <sub>2</sub>                                |   | 10.41                | 7.86  |
| CuCl <sub>2</sub>                               |   | 8.290                | 6.75  |
| CuBr <sub>2</sub>                               |   | 7.589                | 6.37  |
| H   | 7.176   |                      |   |
| Cu(OH) <sub>2</sub>                             |   | 7.540                | 6.66  |
| CuSO <sub>4</sub>                               | 6.219   | 7.540                | 6.70  |
| P   | 5.617   |                      |   |
| Cu <sub>3</sub> (PO <sub>4</sub> ) <sub>2</sub> |   | 7.540                | 6.39  |
| N   | 7.232   |                      |   |
| Cu(NO <sub>3</sub> ) <sub>2</sub>               |   | 7.540                | 7.05  |

#### Appendix D: The variance of the parameters in the fundamental Eq.(1d) depending on the charge of the atom

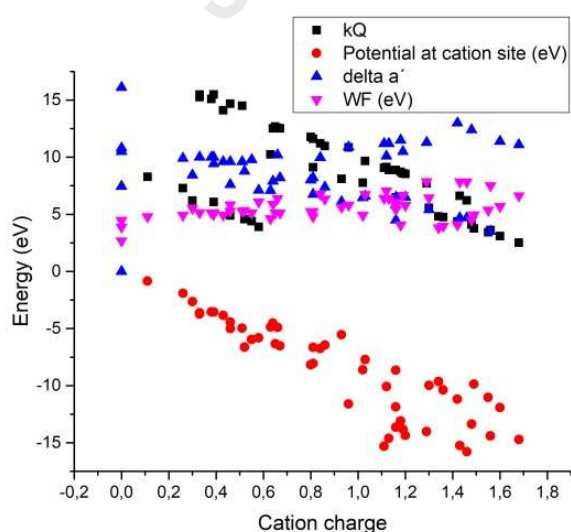


**Fig. 11** General trends of different terms in Eq.(1a) ( $kQ$ ,  $V_M$ ,  $2R(c_i) = \Delta\alpha'$ ,  $\Phi_{\text{solid}} = WF$ ) as a function of the cation charge  $Q_{\text{calc}}$



The plot in Fig.11 summarizes the different ISE and FSE contributions for all compounds discussed here as described in Eq.(1a) in relation to the charges of the cations. The work functions show a small rising trend with growing charge. As expected, both  $kQ$  and  $V_M$  depend strongly on the cation charge. Their variability will therefore dominate the chemical shift in XPS.

The ticks showing the  $kQ$  values are nicely assembled on a line with negative slope with  $ZnF_2$  at its high charge end. In a second line lying a little below we find ticks for Pb compounds and at the highest charges those of the Ba compounds. The Pb compounds have proven to be exceptional due to their specific lone-pair or inert pair electron configuration, and the Ba compounds all excel due to their high ionicity and the high coordination numbers leading to smaller  $k$  values. The  $kQ$  values of Cu(I) compounds are all assembled at lower charges and energies in the range of 4 to 7 eV because there is only 1 valence electron in the game.

The ticks giving the potentials at the cation site (the local Madelung energy) show some spread due to the great differences in the topology of the structures which is also mirrored in the so-called GF factors described above (see section 5.2). However, the general trend of a falling line is clearly seen as expected.

The ticks of the  $\Delta\alpha'$  values as representatives for relaxation effects show two trends, a slightly decreasing line and a second one moving upwards. The former series represent the compounds of Zn, Ba and Pb and also those of Cu(I), whereas the latter one represents the Cu(II) compounds as already discussed above in the context of Fig.9. The open shell configuration is especially noticeable in the relaxation terms, and the extra-atomic part dominates the game. Its contribution to the general term  $R(c)$  grows with increasing charge of the Cu(II) cation making the Auger parameter shift almost independent of the chemical state.

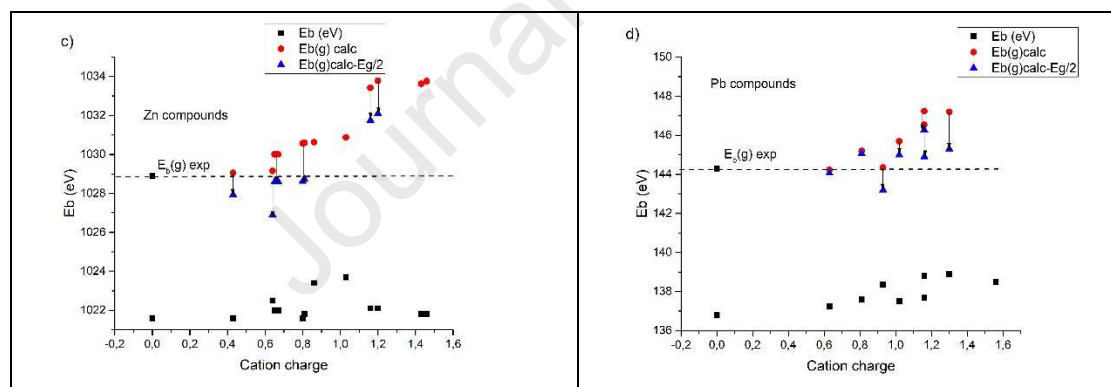
### Appendix E: A comparison of experimental and retro-calculated $E_b(g)$ values

| Compound | $E_b(g)^{exp}$<br>(eV) | $E_b(g)^{retro}$<br>(eV) | $E_g$ [33]<br>(eV) | $E_b(g)^{retro-red}$<br>(eV) | $\Delta^{(retro-red-exp)}$<br>(eV) |
|----------|------------------------|--------------------------|--------------------|------------------------------|------------------------------------|
| $Zn_g$   | 1028.9                 |                          |                    |                              |                                    |
| ZnO-w    |                        | 1033.78                  | 3.35               | 1032.11                      | 3.21                               |
| ZnO-s    |                        | 1033.42                  | 3.35               | 1031.75                      | 2.85                               |
| ZnS-w    |                        | 1030.57                  | 3.91               | 1028.62                      | -0.28                              |
| ZnS-s    |                        | 1030.49                  | 3.54               | 1028.72                      | -0.18                              |
| ZnSe-w   |                        | 1030.01                  | 2.82               | 1028.60                      | -0.3                               |
| ZnSe-s   |                        | 1030.00                  | 2.82               | 1028.59                      | -0.31                              |
| ZnTe     |                        | 1029.05                  | 2.25               | 1027.93                      | -0.97                              |
|          |                        |                          |                    |                              |                                    |
| $Pb_g$   | 144.3                  |                          |                    |                              |                                    |
| PbO-t    |                        | 147.24                   | 1.94               | 146.27                       | 1.9                                |
| PbS      |                        | 145.69                   | 0.41               | 145.49                       | 1.19                               |

|                    |       |        |      |        |       |
|--------------------|-------|--------|------|--------|-------|
| PbSe               |       | 145.20 | 0.27 | 145.07 | 0.71  |
| PbTe               |       | 144.23 | 0.32 | 144.07 | -0.23 |
| PbCl <sub>2</sub>  |       | 147.20 | 3.9  | 145.25 | 0.95  |
| PbBr <sub>2</sub>  |       | 146.54 | 3.2  | 144.94 | 0.64  |
| PbI <sub>2</sub>   |       | 144.35 | 2.32 | 143.19 | -1.1  |
|                    |       |        |      |        |       |
| Cu <sub>g</sub>    | 939.7 |        |      |        |       |
| Cu <sub>2</sub> O  |       | 939.74 | 2.6  | 941.04 | 1.34  |
| Cu <sub>2</sub> S  |       | 938.96 | 1.93 | 939.93 | 0.23  |
| Cu <sub>2</sub> Se |       | 937.17 | 1.23 | 937.79 | -1.91 |
| CuCl               |       | 938.31 | 3.3  | 939.96 | 0.26  |
| CuBr               |       | 937.83 | 3.0  | 939.33 | -0.37 |
| CuI                |       | 937.68 | 3.05 | 939.21 | -0.49 |

The second column shows the measured binding energies  $E_b(g)^{VL}$  for the gaseous elements and the third column gives the value for the retro-calculated ones starting from the binding energies of the respective compounds. The fifth column contains retro-values corrected by subtracting  $\frac{1}{2} E_g$  (for Zn and Pb) or adding this value (for Cu(I)) as given in column four, and the deviations between calculated and experimental values are given in the last column. (See text!)

The experimental and the calculated  $E_b(g)^{VL}$  values agree quite well excepting the Zn-oxides and PbO. (The low  $E_g$  values for ZnO have been questioned in literature. It is known that this compound is non-stoichiometric depending on synthesis, and the same is true for lead chalcogenides. The special feature of PbO is discussed in the closing section of this paper.)



A pictorial comparison of experimental binding energies for gaseous single atoms  $E_b(g)^{VL}$  and the respective values resulting from a retro-calculation for c) Zn and d) Pb compounds (blue triangles). (See text!) The “correction arrows” are shown when band gap values were known.

#### Appendix F: Wagner plots, literature data and comments.

The following tables contain the XPS data reported in the literature for the Ba, Zn, Pb and Cu compounds investigated in this work (In blue colour are evidenced the data employed to draw the Wagner plot).

The work functions for the metals Ba, Pb, Zn and Cu, necessary to change the reference of the binding-energy of core electrons and the kinetic-energy of Auger electrons of the free atoms from the vacuum level to the Fermi level, are obtained from the Handbook of Chemistry and Physics 87th ed. 2006-2007, CRC Taylor and Francis, (D. R. Lide, Editor-in-Chief), p.12-114 :  $\Phi_{Ba(s)} = 2.52$  eV;  $\Phi_{Pb(s)} = 4.25$  eV ;  $\Phi_{Zn(s)} = 3.63$  eV;  $\Phi_{Cu(s)} \approx 5$  eV( this

value was obtained considering the work functions measured on low Miller index crystal faces: (100)  $\Phi_{\text{Cu(s)}} = 5.10$  eV, and (111):  $\Phi_{\text{Cu(s)}} = 4.94$  eV).

The binding-energy and the kinetic-energy data reported in the tables below have been standardized to an energy scale that assumes, with Fermi level referencing, the following binding energies: Au  $4f_{7/2} = 84.0$  eV, Ag  $3d_{5/2} = 368.27$  eV, Cu  $2p_{3/2} = 932.67$  eV, and C  $1s$  (for hydrocarbon or hydrocarbon groups) = 284.8 eV. The C  $1s$  value has been used for the Fermi level referencing of all the insulating samples. The precision of most reported energies is generally not better than 0.1 eV.

### Ba Wagner plot: Ba ( $3d_{5/2}$ ) and Ba ( $M_4N_{45}N_{45}$ )

$$\alpha' = E_b(3d_{5/2}) + E_k(M_4N_{45}N_{45})$$

#### Data from literature:

| References and <b>Compounds</b>   | $3d_{5/2}$ / eV | $M_4N_{45}N_{45}$ / eV | $\alpha'$ / eV | $\Delta\alpha'$ / eV |
|---|-----------------|------------------------|----------------|----------------------|
| a) M. Kellokumpu, H. Aksela, Phys. Rev. A 31 (1985) 777-782;<br>b) A. Mäntykenttä, H. Aksela, S. Aksela, J. Tulkki, T. Åberg, Phys. Rev. A 47 (1993) 4865-4873. |                 |                        |                |                      |
| <b>Ba(g)</b><br>Note: $[E_b(3d_{5/2}) - E_b(4d_{5/2})] = 690.4$ eV.   | 788.7           | 576.8                  | 1365.5         | 0                    |

#### Data from NIST database [11]:

| References and <b>Compounds</b>  | $3d_{5/2}$ / eV | $M_4N_{45}N_{45}$ / eV | $\alpha'$ / eV | $\Delta\alpha'$ / eV |
|--|-----------------|------------------------|----------------|----------------------|
| H. van Doveren, J.A.Th Verhoeven, J. Electron Spectrosc. Relat. Phenom. 21 (1980) 265  |                 |                        |                |                      |
| <b>Ba(s)</b>   | 779.3           | 602.0                  | 1381.3         | 15.8                 |
| <b>BaO</b>   | 779.1           | 598.4                  | 1377.5         | 12.0                 |
| W.V. Lampert, K.D. Rachocki, B.C. Lamartine, T.W. Hass J. Electron Spectrosc. Relat. Phenom. 26 (1982) 133   |                 |                        |                |                      |
| <b>Ba(s)</b>   | 779.8           | 601.9                  | 1381.7         | 16.2                 |
| C.D. Wagner, W.M. Riggs, L.E. Davis, J.F. Moulder, G.E. Muilenberg Handbook of X-Ray Photoelectron Spectroscopy, Perkin-Elmer Corporation, Physical Electronics Division, Eden Prairie, Minn. 55344 (1979) |                 |                        |                |                      |
| <b>BaO</b>   | 779.85          | 597.50                 | 1377.35        | 11.8                 |
| R.P. Vasquez, J. Electron Spectrosc. Relat. Phenom. 56   |                 |                        |                |                      |

|   |       |       |        |      |
|---|-------|-------|--------|------|
| (1991) 217-240.   |       |       |        |      |
| <b>BaS</b>  | 779.3 | 599.2 | 1378.5 | 13.0 |
| <b>BaO</b>  | 779.4 | 597.8 | 1377.2 | 11.7 |
| <b>BaF<sub>2</sub></b>  | 780.0 | 595.8 | 1375.8 | 10.3 |
| <b>BaCl<sub>2</sub></b>   | 780.4 | 596.5 | 1376.9 | 11.4 |
| <b>BaBr<sub>2</sub>·2H<sub>2</sub>O</b>   | 780.4 | 596.8 | 1377.2 | 11.7 |
| <b>BaI<sub>2</sub>·2H<sub>2</sub>O</b>  | 780.6 | 597.3 | 1377.9 | 12.4 |
| The following data have been collected critically by C. D. Wagner in "Practical Surface Analysis" (Second edition), J. Wiley & Sons, Ltd 1990. Appendix 5 Photoelectron and Auger Energies and the Auger Parameter. A Data Set, Barium p.617. |       |       |        |      |
| M.F. Koenig, J.T. Grant, Appl. Surf. Sci. 20 (1985) 481-496.  |       |       |        |      |
| <b>Ba(s)</b><br>Note [ $E_b(3d_{5/2}) - E_b(4d_{5/2})$ ] = 690.4 eV   | 780.6 | 601.0 | 1381.6 | 16.1 |
| <b>BaO</b><br>Note [ $E_b(3d_{5/2}) - E_b(4d_{5/2})$ ] = 690.1 eV.  | 779.9 | 598.0 | 1377.9 | 12.4 |
| H. Seyama, M. Soma, J. Chem. Soc., Faraday Trans. I 80 (1984) 237-248.  |       |       |        |      |
| <b>BaCl<sub>2</sub>·2H<sub>2</sub>O</b>   | 781.6 | 594.9 | 1376.5 | 11.0 |
| <b>BaF<sub>2</sub></b>  | 781.7 | 594.9 | 1376.6 | 11.1 |

### Pb Wagner plot: Pb ( $4f_{7/2}$ ) and Pb ( $N_6O_{45}O_{45}$ )

$$\alpha' = E_b(4f_{7/2}) + E_k(N_6O_{45}O_{45})$$

#### Data from literature:

| References and Compounds   | $4f_{7/2}$ / eV | $N_6O_{45}O_{45}$ / eV | $\alpha'$ / eV | $\Delta\alpha'$ / eV |
|--|-----------------|------------------------|----------------|----------------------|
| M. Patanen, S. Urpelainen, T. Kantia, S. Heinäsmäki, S. Aksela and H. Aksela, Phys. Rev. A 83 (2011) 053408-1-5. |                 |                        |                |                      |
| <b>Pb(g)</b>   | 144.3           | 81.3                   | 225.6          | 0                    |

#### Data from NIST database [11]:

| References and Compounds  | $4f_{7/2}$ / eV | $N_6O_{45}O_{45}$ / eV | $\alpha'$ / eV | $\Delta\alpha'$ / eV |
|---|-----------------|------------------------|----------------|----------------------|
| J. A. Taylor and D. L. Perry, J. Vac. Sci. Technol. A 2 (1984) 771-774. |                 |                        |                |                      |

|   |        |       |        |     |
|---|--------|-------|--------|-----|
| <b>Pb(s)</b>  | 136.7  | 96.3  | 233.0  | 7.4 |
| <b>PbO rhom.</b>  | 137.6  | 92.8  | 230.4  | 4.8 |
| <b>PbO tetra.</b>   | 137.7  | 92.6  | 230.3  | 4.7 |
| C.J. Powell,<br>J. Electron Spectrosc. Relat.<br>Phenom. 185 (2012) 1.  |        |       |        |     |
| <b>Pb(s)</b>  | 136.82 | 95.8  | 232.62 | 7.0 |
| C.D. Wagner, W.M. Riggs, L.E.<br>Davis, J.F. Moulder, G.E.<br>Muilenberg<br>Handbook of X-Ray Photoelectron<br>Spectroscopy, Perkin-Elmer<br>Corporation, Physical Electronics<br>Division, Eden Prairie, Minn.<br>55344 (1979)                                   |        |       |        |     |
| <b>Pb(s)</b>  | 136.80 | 96.25 | 233.05 | 7.5 |
| The following data have been<br>collected critically by C. D. Wagner<br>in "Practical Surface Analysis"<br>(Second edition) , J. Wiley & Sons,<br>Ltd 1990. Appendix 5<br>Photoelectron and Auger Energies<br>and the Auger Parameter. A Data<br>Set, Lead p.623. |        |       |        |     |
| L.R. Pederson, J. Electron<br>Spectrosc. Relat. Phenom. 28<br>(1982) 203-209.   |        |       |        |     |
| <b>Pb(s)</b>  | 136.80 | 96.25 | 233.05 | 7.5 |
| <b>PbTe</b>   | 137.25 | 95.45 | 232.70 | 7.1 |
| <b>PbSe</b>   | 137.60 | 94.75 | 232.35 | 6.8 |
| <b>PbS</b>  | 137.50 | 94.55 | 232.05 | 6.5 |
| <b>PbO</b>  | 137.25 | 92.85 | 230.10 | 4.5 |
| <b>PbI<sub>2</sub></b>  | 138.35 | 93.35 | 231.70 | 6.1 |
| <b>PbBr<sub>2</sub></b>   | 138.8  | 92.6  | 231.4  | 5.8 |
| <b>PbCl<sub>2</sub></b>   | 138.9  | 92.1  | 231.0  | 5.4 |
| <b>PbF<sub>2</sub></b>  | 138.5  | 90.6  | 229.1  | 3.5 |

### Zn Wagner plot Zn (2p<sub>3/2</sub>) and Zn (L<sub>3</sub>M<sub>45</sub>M<sub>45</sub>)

$$\alpha' = E_b(2p_{3/2}) + E_k(L_3M_{45}M_{45} : ^1G)$$

#### Data from literature:

| References and Compounds  | 2p <sub>3/2</sub> / eV | L <sub>3</sub> M <sub>45</sub> M <sub>45</sub> : <sup>1</sup> G / eV | α' / eV | Δα' / eV |
|---|------------------------|--|---------|----------|
| H. Aksela, S. Aksela, H. Patana,<br>Phys. Rev. A 30 (1984) 858. |                        |  |         |          |
| <b>Zn(g)</b>  | 1028.9                 | 974.4  | 2003.3  | 0        |

**Data from NIST database [11]:**

| References and <b>Compounds</b>   | $2p_{3/2}$ / eV | $L_3M_{45}M_{45}$ : $^1G$ / eV | $\alpha'$ / eV | $\Delta\alpha'$ / eV |
|---|-----------------|--------------------------------|----------------|----------------------|
| J.C. Klein and D.M. Hercules<br>J. Catal. 82(1983) 424  |                 |                                |                |                      |
| <b>ZnCl<sub>2</sub></b>   | 1021.9          | 989.4                          | 2011.3         | 8.0                  |
| <b>Zn(s)</b>  | 1021.7          | 992.3                          | 2014.0         | 10.7                 |
| <b>ZnO</b>  | 1021.9          | 988.2                          | 2010.1         | 6.8                  |
| B.R. Strohmeier and D.M.<br>Hercules<br>J. Catal. 86(1984) 266  |                 |                                |                |                      |
| <b>ZnO</b>  | 1021.2          | 988.9                          | 2010.1         | 6.8                  |
| <b>Zn(s)</b>  | 1021.0          | 992.4                          | 2013.4         | 10.1                 |
| <b>ZnS</b>  | 1021.7          | 989.6                          | 2011.3         | 8.0                  |
| S.P. Kowalczyk, L. Ley, F.R.<br>McFeely, R.A. Pollak, D.A.<br>Shirley<br>Phys. Rev.B 9 (1974) 381   |                 |                                |                |                      |
| <b>Zn(s)</b>  | 1021.9          | 991.8                          | 2013.7         | 10.4                 |
| S.P. Kowalczyk, R.A. Pollak,<br>F.R. McFeely, L. Ley, D.A.<br>Shirley<br>Phys. Rev.B 8 (1973) 2387  |                 |                                |                |                      |
| <b>Zn(s)</b>  | 1021.6          | 991.9                          | 2013.5         | 10.2                 |
| G. Schoen<br>J. Electron Spectrosc. Relat.<br>Phenom. 2 (1973) 75.  |                 |                                |                |                      |
| <b>ZnO</b>  | 1021.6          | 988.5                          | 2010.1         | 6.8                  |
| <b>Zn(s)</b>  | 1021.9          | 992.5                          | 2014.4         | 11.1                 |
| C.D. Wagner,<br>Discuss. Faraday Soc. 60 (1975)<br>291  |                 |                                |                |                      |
| <b>ZnF<sub>2</sub></b>  | 1022.8          | 986.7                          | 2009.5         | 6.2                  |
| <b>ZnBr<sub>2</sub></b>   | 1023.4          | 987.3                          | 2010.7         | 7.4                  |
| <b>Zn(s)</b>  | 1021.9          | 992.0                          | 2013.9         | 10.6                 |
| C.D. Wagner, W.M. Riggs, L.E.<br>Davis, J.F. Moulder, G.E.<br>Muilenberg<br>Handbook of X-Ray<br>Photoelectron Spectroscopy,<br>Perkin-Elmer Corporation,<br>Physical Electronics Division,<br>Eden Prairie, Minn. 55344 (1979) |                 |                                |                |                      |
| <b>Zn(s)</b>  | 1021.65         | 992.20                         | 2013.85        | 10.5                 |
| D.W. Langer, C.J. Vesely<br>Phys. Rev.B 2 (1970) 4885   |                 |                                |                |                      |
| <b>ZnO</b>  | 1021.4          | 988.9                          | 2010.3         | 7.0                  |
| <b>ZnS</b>  | 1022.0          | 989.9                          | 2011.9         | 8.6                  |
| <b>ZnSe</b>   | 1021.8          | 988.4                          | 2010.2         | 6.9                  |
| <b>ZnTe</b>   | 1021.6          | 990.6                          | 2012.2         | 8.9                  |

|   |         |        |         |      |
|---|---------|--------|---------|------|
| J.M. Mariot, G. Dufour<br>Chem. Phys. Lett. 50 (1977) 219   |         |        |         |      |
| <b>Zn(s)</b>  | 1021.6  | 992.3  | 2013.9  | 10.6 |
| C.J. Powell,<br>J. Electron Spectrosc. Relat.<br>Phenom. 185 (2012) 1; 182<br>(2010) 11   |         |        |         |      |
| <b>Zn(s)</b>  | 1021.76 | 992.40 | 2014.16 | 10.9 |
| P.S. Wehner, P.N. Mercer, G.<br>Apai<br>J. Catal. 84 (1983) 244   |         |        |         |      |
| <b>ZnO</b>  | 1022.0  | 988.1  | 2010.1  | 6.8  |
| <b>Zn(s)</b>  | 1021.7  | 992.1  | 2013.8  | 10.5 |
| T.D. Thomas and P. Weightman<br>Phys. Rev. B 33 (1986) 5406   |         |        |         |      |
| <b>Zn(s)</b>  | 1021.60 | 992.22 | 2013.82 | 10.5 |
| R. Islam and D.R. Rao<br>J. Electron Spectrosc. Relat.<br>Phenom. 81 (1996) 69.   |         |        |         |      |
| <b>ZnSe</b>   | 1022.2  | 989.1  | 2011.3  | 8.0  |
| L.S. Dake, D.R. Baer, J.M.<br>Zachara<br>Surf. Interface Anal. 14 (1989) 71   |         |        |         |      |
| <b>ZnO</b>  | 1022.3  | 988.1  | 2010.4  | 7.1  |
| <b>ZnS sphalerite</b>   | 1021.8  | 989.7  | 2011.5  | 8.2  |
| <b>ZnS sphalerite</b>   | 1021.8  | 989.8  | 2011.6  | 8.3  |
| <b>ZnCl<sub>2</sub></b>   | 1023.7  | 986.2  | 2009.9  | 6.6  |
| <b>Zn(s)</b>  | 1021.6  | 992.2  | 2013.8  | 10.5 |
| G. Deroubaix and P. Marcus<br>Surf. Interface Anal. 18(1992) 39   |         |        |         |      |
| <b>ZnS</b>  | 1022.0  | 989.4  | 2011.4  | 8.1  |
| <b>ZnO</b>  | 1022.1  | 988.2  | 2010.3  | 7.0  |
| <b>Zn(s)</b>  | 1021.8  | 992.1  | 2013.9  | 10.6 |
| The following data have been<br>collected critically by C. D.<br>Wagner in "Practical Surface<br>Analysis" (Second edition) , J.<br>Wiley & Sons, Ltd 1990.<br>Appendix 5 Photoelectron and<br>Auger Energies and the Auger<br>Parameter. A Data Set, Zinc<br>pp.608-609. |         |        |         |      |
| R. Hoogewijs, L. Fiermans and J.<br>Vennik, J. Electron Spectrosc.<br>Relat. Phenom. 11 (1977) 171  |         |        |         |      |
| <b>ZnTe</b>   | 1021.6  | 991.3  | 2012.9  | 9.6  |
| <b>ZnSe</b>   | 1022.0  | 989.5  | 2011.5  | 8.2  |
| S.W. Gaarenstroom and N.<br>Winograd, J. Chem. Phys. 67<br>(1977) 3500  |         |        |         |      |

|  |        |       |        |      |
|--|--------|-------|--------|------|
| <b>ZnS</b>                                   | 1021.6 | 989.7 | 2011.3 | 8.0  |
| <b>ZnO</b>                                   | 1022.1 | 987.7 | 2009.8 | 6.5  |
| <b>ZnI<sub>2</sub></b>                       | 1022.5 | 988.7 | 2011.2 | 7.9  |
| <b>ZnF<sub>2</sub></b>                       | 1021.8 | 986.2 | 2008.0 | 4.7  |
| S. Evans, Surf. Interface Anal. 7 (1985) 299 |        |       |        |      |
| <b>Zn(s)</b>                                 | 1021.7 | 992.1 | 2013.8 | 10.5 |

### Cu Wagner plot Cu (p<sub>3/2</sub>) and Cu (L<sub>3</sub>M<sub>45</sub>M<sub>45</sub>)

$$\alpha' = E_b(2p_{3/2}) + E_k(L_3M_{45}M_{45} : ^1G)$$

#### Data from literature:

| References and <b>Compounds</b>   | 2p <sub>3/2</sub> / eV | L <sub>3</sub> M <sub>45</sub> M <sub>45</sub> : <sup>1</sup> G / eV | $\alpha'$ / eV | $\Delta\alpha'$ / eV |
|---|------------------------|--|----------------|----------------------|
| S. Aksela, J. Sivonen, Phys. Rev. A 25 (1982) 1243.<br>H. Aksela, S. Aksela, H. Patana, Phys. Rev. A 30 (1984) 858. |                        |  |                |                      |
| <b>Cu(g)</b>  | 939.7                  | 900.7  | 1840.4         | 0                    |
| M.C. Biesinger, Surf. Interface Anal. 49 (2017) 1325.   |                        |  |                |                      |
| <b>Cu<sub>2</sub>O</b>  | 932.18                 | 916.99   | 1849.17        | 8.8                  |
| <b>CuCl</b>   | 932.34                 | 915.18   | 1847.51        | 7.1                  |
| <b>CuBr</b>   | 932.27                 | 915.72   | 1848.00        | 7.6                  |
| <b>CuI</b>  | 932.50                 | 916.34   | 1848.84        | 8.4                  |
| <b>CuFeS<sub>2</sub></b>  | 932.14                 | 918.04   | 1850.18        | 9.8                  |
| <b>Cu<sub>2</sub>S</b>  | 932.62                 | 917.23   | 1849.84        | 9.4                  |
| <b>CuO</b>  | 933.76                 | 917.57   | 1851.33        | 10.9                 |
| <b>CuF<sub>2</sub></b>  | 936.38                 | 915.36   | 1851.74        | 11.3                 |
| <b>CuCl<sub>2</sub></b>   | 935.30                 | 915.08   | 1850.37        | 10.0                 |
| <b>CuBr<sub>2</sub></b>   | 934.50                 | 916.10   | 1850.60        | 10.2                 |
| <b>Cu(OH)<sub>2</sub></b>   | 934.67                 | 916.25   | 1850.92        | 10.5                 |
| <b>CuSO<sub>4</sub></b>   | 936.00                 | 915.91   | 1851.91        | 11.4                 |
| <b>Cu<sub>3</sub>(PO<sub>4</sub>)<sub>2</sub></b>   | 935.85                 | 915.76   | 1851.61        | 11.2                 |
| <b>Cu(NO<sub>3</sub>)<sub>2</sub>•3H<sub>2</sub>O</b>   | 935.51                 | 914.98   | 1850.49        | 10.1                 |
| <b>Cu(s)</b>  | 932.63                 | 918.61   | 1851.24        | 10.8                 |

#### Data from NIST database [11]:

| References and <b>Compounds</b>  | 2p <sub>3/2</sub> / eV | L <sub>3</sub> M <sub>45</sub> M <sub>45</sub> : <sup>1</sup> G / eV | $\alpha'$ / eV | $\Delta\alpha'$ / eV |
|--|------------------------|--|----------------|----------------------|
| R. Romand, M. Roubin and J. P. Deloume, Electron Spectrosc. Relat. Phenom. 13 (1978) 229 |                        |  |                |                      |
| <b>CuSe</b>  | 932.0                  | 918.4  | 1850.4         | 10.0                 |
| D. Cahen, D. J. Ireland, L.L. Kazmerski and F.A. Thiel, J. Appl. Phys. 57(1985) 4761     |                        |  |                |                      |



|  |       |       |        |     |
|--|-------|-------|--------|-----|
| <b>Cu<sub>2</sub>Se</b>  | 932.5 | 917.8 | 1850.3 | 9.9 |
| D.L. Perry and J.A. Taylor, J. Mat. Sci. Letters 5 (1986) 384.   |       |       |        |     |
| <b>Cu<sub>2</sub>S (chalcocite)</b>  | 932.4 | 917.5 | 1849.9 | 9.5 |
| <b>CuS (covellite)</b>   | 932.2 | 918.1 | 1850.3 | 9.9 |
| The following data has been collected critically by C. D. Wagner in "Practical Surface Analysis" (Second edition), J. Wiley & Sons, Ltd 1990. Appendix 5 Photoelectron and Auger Energies and the Auger Parameter. A Data Set, Cu p.608. |       |       |        |     |
| R. Romand, M. Roubin and J. P. Deloume, Electron Spectrosc. Relat. Phenom. 13 (1978) 229   |       |       |        |     |
| <b>Cu<sub>2</sub>Se</b>  | 931.9 | 917.6 | 1849.5 | 9.1 |

## Highlights

We discuss factors determining chemical shifts of measured binding energies in XPS in a unifying equation, and we quantify different factors separately which bias the measurement of the kinetic energies of the outgoing electrons.

We present a theory combining several parameters resulting from DFT calculations which will influence the energy of photoelectrons and we thereby help to rationalize the scatter of data points in diverse presentations such as Wagner plots. .

We show how Bader charges and basin volumes resulting from DFT calculations as well as site potentials give a data basis to rationalize the spread of measured binding energies and Auger parameters.

We demonstrate how the structural topology of a crystalline solid is mapped in the variations of the kinetic energy of photoelectrons.

We show how an estimate of work functions resulting from Mulliken electronegativities can be included in such a unifying approach and how even types of semiconductors can be foreseen.

There is no additional statement other than the items given in the separate letter to the editor.

Journal Pre-proof

There is no conflict of interest whatsoever.

Journal Pre-proof